Caudal *Fgfr1* disruption produces localised spinal mis-patterning and a terminal myelocystocele-like phenotype in mice

Eirini Maniou[1,2,*], Faduma Farah[1], Abigail R. Marshall[1], Zoe Crane-Smith[1], Andrea Krstevski[1], Athanasia Stathopoulou[1], Nicholas D.E. Greene[1], Andrew J. Copp[1], Gabriel L. Galea[1,*]

[1]Developmental Biology and Cancer Department, UCL GOS Institute of Child Health, London, UK
[2]Present address: Department of Industrial Engineering, University of Padova, Padova, Italy

*Corresponding authors: e.maniou@ucl.ac.uk and g.galea@ucl.ac.uk

Summary statement

Conditional deletion of *Fgfr1* prevents formation of the posterior neuropore caudal closure site, Closure 5, delaying spinal neural tube closure, and phenocopies the closed spinal dysraphism 'terminal myelocystocele' in mice.

Abstract

Closed spinal dysraphisms are poorly understood malformations classified as neural tube (NT) defects. Several, including terminal myelocystocele, affect the low spine. We previously identified a NT closure-initiating point, Closure 5, in the distal spine of mice. Here we document equivalent morphology of the caudal-most closing posterior neuropore (PNP) in mice and humans. Closure 5 forms in a region of active FGF signalling and pharmacological FGF receptor blockade impairs its formation in cultured mouse embryos. Conditional genetic deletion of *Fgfr1* in caudal embryonic tissues with *Cdx2*^{Cre} diminishes neuroepithelial proliferation, impairs Closure 5 formation and delays PNP closure. After closure, the distal NT of *Fgfr1*-disrupted embryos dilates to form a fluid-filled sac overlying ventrally flattened spinal cord. This phenotype resembles terminal myelocystocele. Histological analysis reveals regional and progressive loss of SHH and FOXA2-positive ventral NT domains, resulting in OLIG2-labelling of the ventral-most NT. The OLIG2-domain is also subsequently lost, eventually producing a NT entirely positive for the dorsal marker PAX3. Thus, a terminal myelocystocele-like phenotype

can arise after completion of NT closure with localised spinal mis-patterning caused by disruption of FGFR1 signalling.

Keywords: Neural tube, FGFR1, terminal myelocystocele, patterning

Introduction

Neural tube defects (NTDs) are a heterogenous group of congenital malformations resulting from dysmorphogenesis of the neural tube (NT), the embryonic precursor of the central nervous system. The most common and severe NTDs are those caused by failure to close the NT, including open spina bifida (myelomeningocele). Successful closure of the NT during primary neurulation requires coordinated deformation of the neural plate into a continuous tube of neuroepithelial cells covered by surface ectoderm along the back of the embryo (1). Closure begins at distinct closure-initiating points where the opposite neural folds are first brought into apposition at the dorsal midline. Five closure-initiating points had originally been proposed to initiate NT closure, based on anatomical clustering patterns of NTD lesions in human embryos (2, 3). Three closure-initiating points were subsequently experimentally identified in mouse embryos: Closure 1 at the hindbrain/cervical boundary, Closure 2 at the forebrain/midbrain boundary (absent in humans) and Closure 3 at the ventral forebrain (4). The regions of open NT between these Closure points, called neuropores, close through progressive zippering (1). No closure-initiating point is present where Closure 4 was initially inferred, but we have more recently confirmed the presence of Closure 5 at the end of the presumptive spinal NT in mice (5, 6). Closure 5 is a load-bearing tissue structure which physically holds the neural folds together at the dorsal midline during an approximately 10-hour period from when it is first morphologically identifiable (~25 somite stage) until the spinal NT is fully closed (~30 somite stage). This ephemeral structure has not yet been visualised in human embryos.

In mice, surface ectoderm cells at Closure 5 extend cellular ruffles, consistent with zippering in a caudal-to-cranial direction (5). Thus, the presumptive spinal neuropore, called the posterior neuropore (PNP), closes primarily due to caudally-directed zippering from Closure 1, biomechanically aided at late stages by Closure 5. After completion of PNP closure, the NT lumen extends caudally beyond Closure 5 through a process of mesenchyme-to-epithelium transition with lumen formation referred to as secondary neurulation, forming the sacral and

coccygeal spine. Several important but poorly understood NTDs characteristically localise to the junctional region between primary and secondary neurulation, where Closure 5 forms (7, 8). These include terminal myelocystocele, often described as a “closed” form of spina bifida because the dysmorphic spinal cord is covered with skin (9). Terminal myelocystocele characteristically presents as a trumpet-like flaring of the spinal cord’s distal central canal, forming a localised cystic dilation at the terminal end of the body which continues to expand postnatally (9, 10). It is commonly associated with other malformations, including of musculoskeletal and urogenital structures, and variable neurological dysfunction (10).

There are, to our knowledge, no established animal models of terminal myelocystocele which mechanistically explain its pathogenesis. The most widely-cited hypothesis for its formation relates to a balloon-like dilation observed at the junction between the primary and secondary NT of chick embryos (9), although this is an aspect of normal neurulation and is not a pathological finding. The joined primary and secondary NT form a continuous lumen bordered by neuroepithelial cells which differentiate into dorsoventrally patterned neural lineages. Many progenitor domains are similar between the primary and secondary NT, including a dorsal PAX3-expressing domain, intermediate PAX6 domain and ventral FOXA2 domain (11). However, there are regional differences in neural patterning including the absence of motor neuron differentiation in the caudal NT region formed through secondary neurulation (11). Motor neuron progenitors (pMN) differentiate in the ventral primary NT and are characteristically identified by expression of the transcription factor OLIG2, promoted by high levels of Sonic hedgehog (SHH) morphogen from the NT floorplate and underlying notochord (12, 13). SHH is the best-established inducer of ventral NT fates (14, 15), but does not act in isolation. For example, fibroblast growth factor (FGF) ligands promote maintenance of spinal neural progenitor identities while restricting differentiation into post-mitotic neurons (16-18). FGF signalling opposes somitic mesoderm-derived retinoic acid, which promotes neuron terminal differentiation in part by down-regulating *Fgf8* (19-21). Loss of the retinoic acid synthesising enzyme *Raldh2* does not prevent neuroepithelial commitment, as shown by SOX2 expression, but impairs differentiation of dorsoventral progenitor domains including ventral OLIG2 and intermediate PAX6 in mice (22).

Insults which change the timing of neural progenitor differentiation have also been associated with open spina bifida in mice, such as loss of the dorsal neural tube marker PAX3 (23, 24) or unrepressed SHH signalling causing expansion of ventral neural tube fates (25, 26). Studies into the interplay between neurulation and subsequent neurogenesis have been limited by the

severely abnormal morphology of embryos lacking key mediators. For example, embryos globally lacking the FGF receptor FGFR1 die soon after gastrulation without closing any portion of their NT (27). FGF pathway components including ligands such as neuroepithelial FGF8 are particularly enriched in the caudal-most part of embryo, where Closure 5 forms (28).

Here we initially used a combination of pharmacological antagonism and regional genetic deletion to test the contributions of FGF signalling, specifically through FGFR1, in PNP closure and Closure 5 formation. Conditional genetic deletion of *Fgfr1* produces mouse fetuses which are viable until birth but have a cystic dilation of the distal spinal NT forming a closed spinal dysraphism. We find that the embryological origins of this malformation involve regional and progressive loss of NT ventral progenitor domains prior to the closed and dorsalised NT flattening ventrally while retaining its dorsal skin covering, closely resembling terminal myelocystocele in humans.

Results

Gradual neural fold elevation forms Closure 5 at late stages of spinal closure

Human primary neurulation is completed by Carnegie Stage (CS)13, around 30-35 days of gestation (29). At CS11, the PNP is open and has a spade-like morphology (Figure 1A) equivalent to the mouse PNP on embryonic day E9.5 (Figure 1B). Progression of mouse PNP closure involves caudal narrowing to form an elliptical opening surrounded by purse string-like F-actin cables as Closure 5 forms at the PNP's caudal extreme (Figure 1B). Although late-stage human PNPs are not available to us for 3D imaging, brightfield images archived by the Human Developmental Biology Resource suggest equivalent changes in shape to form an elliptical PNP with caudal Closure 5 in humans as in mice (Supplementary Figure 1).

We previously demonstrated that Closure 5 is a load-bearing structure (5, 6). Here we observe that it forms through gradual elevation of the caudal neural fold tips. The caudal PNP neuroepithelium is everted at earlier developmental stages, but progressively becomes apically concave as the neural fold tips elevate dorsally in embryos with more than 25 somites (Figure 1C-E), when Closure 5 typically forms. Dorsal elevation of the rostral zippering point follows an inverse pattern: it is initially elevated ~200 µm above the ventral-most apical neuroepithelium, but its elevation halves to ~100 µm in later-stage embryos with established Closure 5 (Figure

1E). The continuum of neural fold morphologies, from early eversion to late elevation, suggests coordinated morphogenesis of the caudal PNP to complete primary neurulation.

Pharmacological blockade of FGF signalling diminishes Closure 5 formation

The caudal PNP is known to be enriched in components of cascades including canonical Wnt and FGF signalling (Supplementary Figure 2). FGF components are particularly prominent (Supplementary Figure 2) and we observe marked phosphorylation of the pathway's putative down-steam effector ERK1/2 selectively around Closure 5 (Figure 1F). Phosphorylated FGFR1 is present diffusely around the PNP, particularly in the cytoplasm of mitotic cells (Supplementary Figure 3A), and its staining intensity is reduced in embryos treated for 24 hours with the pan-FGFR inhibitor BGJ 398 (Supplementary Figure 3B). Pharmacological inhibition of FGFR signalling in mouse whole embryo culture causes PNP morphology to become highly irregular, particularly in the caudal-most PNP where abnormal tissue outgrowth forms instead of Closure 5 (Figure 1G). This inhibitor does not change somite gain (vehicle 27±3 somites, pan-FGFR inhibitor 26±3 somites at the end of culture, mean±SD), but produces larger somites (Supplementary Figure 4).

The range of PNP morphologies observed in FGFR-inhibited embryos suggests abnormal progression of closure (Supplementary Figure 5A). Cells within this outgrowth are derived from neuromesodermal progenitors lineage-traced with $T^{CreERT2}$, which continues to lineage-trace both neural tube and mesoderm cells after 24 hours of FGFR inhibition (Supplementary Figure 5B). Cells in the PNP outgrowth also continue to express the neuroepithelial marker N-cadherin (Supplementary Figure 5C).

Phosphorylation of ERK1/2 around the PNP rim persists despite FGFR inhibition (Figure 2A), suggesting activation through other mechanisms, different phosphorylation stabilities or distinct regulatory feedback mechanisms. Expression of the pathway ligand *Fgf8* is retained or increased in the PNP neuroepithelium, whereas it is abolished in the forelimb bud of FGFR-inhibited embryos (Figure 2B, Supplementary Figure 6A), indicating tissue-specific regulation. Retinoic acid signalling is known to interact mutually-antagonistically with caudally-active FGF signalling (21, 30). Pharmacological FGFR blockage causes caudal expansion of the retinoic acid signalling domain genetically labelled with a retinoic acid response element (RARE) driving LacZ expression. RARE caudal expansion is observed within 8 hours of FGFR inhibition, before the PNP is morphologically abnormal (Supplementary Figure 6B-C), and persists after 24 hours

of inhibition (Figure 2C-D). However, RARE activity does not detectably extend to the caudal-most PNP region where Closure 5 should form (Figure 2C). The caudal PNP fails to elevate, remaining everted, in contrast to vehicle-treated controls which elevate their caudal PNP beyond the 25 somite stage (Supplementary Figure 7A-B). FGFR inhibitor-treated embryos largely fail to form Closure 5 and do not complete PNP closure by E10.5 (Supplementary Figure 7C).

Various FGF receptors are known to be expressed in and around the PNP and may have both redundant and obligate roles. *Fgfr3* knockout causes post-natal phenotypes without NTDs (31). *Fgfr2* embryos die ~E11.5, after successful closure of the neural tube (32). *Fgfr1* is expressed diffusely around the PNP rim (Figure 2E) (33) and its chimeric deletion causes distal spina bifida (34). We therefore focused on *Fgfr1* as the more likely non-redundant mediator of FGF signalling promoting PNP closure. Treating cultured embryos with a second, FGFR1-targeting pharmacological antagonist PD 173074 (35, 36) similarly caused neuroepithelial outgrowth, failure of caudal elevation and failure of Closure 5 formation (Figure 2F-G). This second antagonist also did not change somite gain (vehicle 28±3 somites, FGFR1-targeting inhibitor 29±2 somites at the end of culture, mean±SD) and unlike the previously used inhibitor it did not change somite size (Supplementary Figure 4).

Fgfr1 conditional deletion prevents Closure 5 formation, but does not stop spinal closure

Given inherent limitations of pharmacological antagonists we sought to genetically delete *Fgfr1* in all tissues potentially involved in Closure 5 formation while avoiding early lethality seen in global knockouts (37, 38). This was achieved using paternally-inherited CDX2P-NLS Cre (39) (henceforth $Cdx2^{Cre}$) driving deletion of a previously-reported (38) *Fgfr1* conditional allele ($Fgfr1^{Fl/Fl}$). $Cdx2^{Cre}$ recombines in all embryonic tissues caudal to the cervical spine with some notable exceptions: at E10.5 it does not recombine in the notochord or lateral plate mesoderm (Figure 3A-B). Heterozygous $Cdx2^{Cre/+}Fgfr1^{Fl/+}$ (henceforth Cre;Fl/+) mice are viable and fertile. Embryos with this genotype are morphologically indistinguishable from their Cre-negative littermates and are therefore included as ‘controls’. Homozygous $Cdx2^{Cre/+}Fgfr1^{Fl/Fl}$ (henceforth Cre;Fl/Fl) embryos appear caudally truncated, with an open PNP at E10.5 (Figure 3A,C). Loss of *Fgfr1* does not impair embryo growth between the forelimb and hindlimb buds, but selectively truncates caudal elongation from the hind limbs to the end of the body (Figure 3B). At this stage

their PNP is irregularly shaped with corrugated neuroepithelium (Figure 3C-D), reminiscent of FGFR antagonist-treated embryos in culture.

Fgfr1 conditional deletion significantly diminishes proliferation of neuroepithelial cells, but not of mesodermal or hindgut cells, and does not substantially alter apoptosis in these tissues in the distal trunk of E10.5 embryos (Supplementary Figure 8A-E). To further explore the impact of *Fgfr1* loss of neuroepithelial proliferation we analysed embryos at early (E9.5) and late (E10.5) stages of PNP closure. *Fgfr1* conditional deletion diminished the number of mitotic figures in the neuroepithelium at both timepoints (Supplementary Figure 8F-G). Cre;Fl/Fl embryos continue to assemble long F-actin cables bordering the PNP as seen in wild-type embryos, and achieve progressive shortening of the PNP (Figure 3D,E). The caudal PNP elevates progressively in control embryos, whereas in Cre;Fl/Fl it tends to become increasingly everted (Figure 3F). Consequently, in embryos with >25 somites, 43% of control embryos have a PNP morphology indicative of Closure 5, compared with only 8.3% of Cre;Fl/Fl embryos (Figure 3G). Thus, caudal deletion of *Fgfr1* causes morphologically abnormal PNPs which typically lack Closure 5 formation.

At this stage of development, the domain of *Fgf8* expression appears expanded in Cre;Fl/Fl embryos compared with littermate controls (Supplementary Figure 9A), as had been seen following pharmacological FGFR inhibition.

Fgfr1 **disruption causes a terminal myelocystocele-like phenotype**

A significantly smaller proportion of Cre:Fl/Fl than control embryos achieve PNP closure by E10.5 and a sub-set remain open at E11.5 (Figure 4A), exhibiting open lesions caudal to the hind limb buds (Supplementary Figure 9B), whereas all control embryos close their PNP by this timepoint (Figure 4B). All fetuses collected from E12.5 onwards had closed neural tubes (Figure 4A), defined as surface ectoderm/skin fully covering the developing spinal cord. Control embryos at E11.5 have a closed quasi-cylindrical neural tube extending past paired somites into the tail bud (Figure 4B). Somites flanking the closed neural tube within the embryonic tail are markedly hypoplastic in Cre;Fl/Fl embryos (Figure 4B). Hypoplastic somites may result in impaired synthesis of retinoic acid lateral to the neural tube as these structures normally express the retinoic acid synthesising enzyme RALDH2 (Supplementary Figure 10A).

At E12.5, Cre:Fl/Fl embryos develop a cystic dilation of the neural tube lumen selectively between the hindlimbs (Figure 4C-D). Serial cross-sections reveal a trumpet-like flaring of the central canal with a thin dorsal neuroepithelium overlying the dilated portion (Figure 4D). By E14.5 the dorsal thinning of the roof plate and canal dilation progresses to form a ventrally-flattened spinal cord which has an 'open' morphology, yet is covered by skin overlying a fluid-filled sac (Figure 4E-F). This sac-like lesion at the end of the spinal cord morphologically resembles terminal myelocystocele lesions. Additional malformations are evident in these fetuses, including absence of the ventral vertebral body (Figure 4F), limb malformations and apparent delay in perineal fusion (Supplementary Figure 10B-C).

We immunolabelled neural progenitors to confirm the identity of cells in the misshapen spinal cord of Cre;Fl/Fl embryos. SOX2 labels a continuous neuroepithelial layer encircling the central canal, but this layer is thinned dorsally in Cre;Fl/Fl embryos at E14.5 (Figure 5A). This dorsal neuroepithelium lies ventral to the overlying skin layer which stains positively for E-cadherin (Figure 5A). This dysmorphology arises in a region of closed neural tube between the hindlimb buds which is morphologically normal at E11.5 (Figure 5B). At this stage, HUC/D and TUJ1 positive neurons are specified in both control and Cre;Fl/Fl embryos (Figure 5B-D). The ratio of SOX2-positive to HUC/D-positive cells along the lateral neural tube is not significantly different between control and Cre;Fl/Fl embryos (Supplementary Figure 11A-B). Dorsal views of the neural tube show distinct parallel populations of TUJ1 positive neurons extending projections between the hind limb buds in both, but more prominently in Cre;Fl/Fl than control embryos (Figure 5D) potentially due to hypoplasia of surrounding tissues making these neurons more readily visible.

Regional neural tube dorsalisation precedes cystic dilation

FGF signalling has previously been found to maintain neuroepithelial cells in a progenitor state while reducing their terminal differentiation (18). Cross-sections through the lumbar neural tube of Cre;Fl/Fl embryos at E11.5 reveal distinct ventral (SHH, FOXA2, OLIG2: Supplementary Figure 12A,B) and dorsal (PAX3: Supplementary Figure 12C) progenitor domains within the neural tube. Migrating neural crest cells, labelled with SOX9, can readily be identified in streams lateral to the neural tube of Cre;Fl/Fl embryos (Supplementary Figure 12C). PAX3 also immunolabels paraxial mesoderm (dermomyotome), which is markedly smaller in *Fgfr1*-disrupted embryos (Supplementary Figure 12C).

Fgfr1 disruption causes progressive abnormalities of spinal progenitor domains. Cre;Fl/Fl embryos commonly have ectopic clusters of cells ventral to and distinct from the neural tube. These clusters express SOX2 (Figure 5B,C), confirming their neuroepithelial identity, as well as SHH (Figure 6A), FOXA2 (Supplementary Figure 12B), and appear to produce TUJ1-positive axonal projections (Figure 6A). They are identifiable in a short region of the neural tube between the hindlimbs and may act as an ectopic source of SHH when present alongside the floorplate and notochord (Supplementary Figure 12D). However, SHH-expressing ectopic clusters are also observable adjacent to locations devoid of detectable SHH in the ventral neural tube (Figure 6A).

Regional loss of floorplate markers is observable in *Fgfr1*-disrupted embryos as early as E10.5 (Figure 6B), initially replaced by ventral extension of the OLIG2 domain between the hindlimb buds (Supplementary Figure 12E). By E11.5, even the OLIG2 domain is progressively lost as the intermediate PAX6 domain expands ventrally (Figure 6C). At more caudal levels within the same embryo, the dorsal PAX3 domain extends along the entire dorso-ventral axis of the NT (Figure 6C). PAX3 immunolabels the entire NT as it becomes abnormally circular in shape more caudally (Supplementary Figure 13A). Thus, ectopic ventral neuroepithelial clusters and progressive loss of ventral neural progenitor identities precedes NT dysmorphology which produces a terminal myelocystocele-like cystic dilation of the lumen predictably at the terminal end of the embryo (Supplementary Figure 13B).

Discussion

The embryological origins of closed NTD sub-types have largely been inferred from their post-natal morphology and location. Animal models have been invaluable in identifying genetic/teratogenic causes of open NTDs (40), testing putative preventative agents (41), and even paving the way for spina bifida fetal surgery (42), but such models are lacking for most cases of closed NTDs. Here, we show that the human closing PNP is morphologically analogous to that of mouse embryos, and provide brightfield images suggesting it similarly adopts an elliptical structure with terminal Closure 5 at late stages of closure. The seemingly linear elevation of the caudal PNP neural folds with advancing somite stage suggests Closure 5 formation is a coordinated shape change starting at least a day earlier in mouse development.

We had previously reported impaired caudal neural fold elevation and abnormal Closure 5 associated with a caudal tissue ‘bulge’ in a model of conditional *Vangl2* deletion (6). We now

observe a more exophytic outgrowth of caudal neuroepithelium where Closure 5 should have formed in embryos with pharmacologically-inhibited FGF signalling. While we do not provide a definitive explanation for this outgrowth phenotype, it may involve overactivation of retinoic acid signalling, compensatory up-regulation of pathway components as indicated by increased *Fgf8* seen in our pharmacological and genetic models, and/or altered interactions between the neuroepithelium and paraxial mesoderm. After gastrulation, mesoderm and neuroepithelium share a *T*-expressing neuromesodermal progenitor population. FGF signalling has been suggested to maintain and direct differentiation of this progenitor pool (43, 44). However, we do not observe gross cessation of contributions from this lineage to either neuroepithelial or mesodermal tissues within a 24-hour period of FGF antagonism in whole embryo culture.

Neuromesodermal progenitors contribute to axial elongation (45), for which FGF signalling is critically required (46). This is consistent with our observation of caudal truncation in embryos with caudally deleted *Fgfr1*, suggesting a non-redundant role for this receptor in axial elongation beyond the hindlimbs. Diminished neuroepithelial proliferation observed following deletion of *Fgfr1* is consistent with this pathway's known mitogenic effects on neural progenitors (47, 48). Truncal elongation is unaffected despite being within the recombination domain of $Cdx2^{Cre}$, suggesting receptor redundancy or activation of compensatory mechanisms which are well-described for this complex pathway (49). The concordance between failure of caudal PNP elevation and lack of Closure 5 formation seen with pharmacological antagonism of FGF receptors and selective genetic deletion of *Fgfr1* corroborates our hypothesis that completion of PNP closure selectively requires this receptor. The neural tube phenotypes we observe when using two different FGFR-targeting antagonists are very similar, but only the pan-FGFR inhibitor produces larger somites. An increase in somite size had previously been reported following pan-FGFR inhibition in chick embryos (50). Absence of this somite phenotype when mouse embryos are cultured in the FGFR1-targeting antagonist used here may reflect differential tissue penetration, compound duration of action, or FGFR1-independent mechanisms in mice. The latter explanation is consistent with our observations of smaller somites in embryos with genetic deletion of *Fgfr1* at later stages.

FGFR pharmacological antagonists are also known to have off-target effects including on VEGF receptors and SRC. However, both the antagonists used in this study and *Fgfr1* genetic deletion produced highly corrugated neuroepithelium at late stages of PNP closure. In-folding might produce the clusters of neuroepithelial cells observed in cross-section after the neural tube has closed in our *Fgfr1*-deletion model. Identifying the specific cell types in which *Fgfr1* signalling

promotes neural fold elevation will require future tissue-specific deletion studies. Previous studies which deleted *Fgfr1* using T^{Cre} reported musculoskeletal phenotypes comparable to those observed here, but not PNP dysmorphology or later terminal myelocystocele-like phenotypes (33, 51). Similarly, $Pax3^{Cre}$ deletion of *Fgfr1* caused kidney malformation, but neural tube defects were not reported (52). It is not clear whether neural tube phenotypes were carefully assessed in those studies. $Cdx2^{Cre}$ used in this study provides near-global gene deletion in caudal embryonic tissues which starts sufficiently late in development to avoid lethality, yet sufficiently early to impact completion of neural tube closure. We observe that $Cdx2^{Cre}$ does not recombine in the notochord: whether persistent FGFR1 signalling in this tissue contributes to the phenotypes observed remains to be determined.

The ability of embryos with caudally deleted *Fgfr1* to achieve delayed yet complete PNP closure is surprising, not only because of the level of dysmorphology their closure process overcomes, but also because alternative disruptions of the same gene cause open spina bifida in mice. Chimeric embryos containing *Fgfr1*-null cells develop spina bifida in a proportion of cases (34). Embryos in which exon 3 of *Fgfr1* is globally deleted, preventing expression of the *Fgfr1α* isoform, also develop fully penetrant spina bifida, confounded by severe dysmorphology and early lethality (53). A hypomorphic *Fgfr1* allele has also been reported to cause spina bifida and skeletal malformations similar to those reported here (47). In the current study we delete exons 8-14 (38), which include the transmembrane domain common to all isoforms (54), yet only produce closed spinal lesions at late stages of development. The open spinal neural tube we observed in a subset of embryos at E11.5 suggests predisposition to open spina bifida in our model which is not manifest in the environment and genetic background tested. Shared genetic basis between open and closed NTDs has previously been reported in the cranial region for exencephaly and encephalocele (55).

Closed NTD-like phenotypes have been reported in a few other models. Deletion of the FGFR1 receptor specific subtrate (Frs) causes similar dilation of the distal neural tube in mouse embryos (56). A small, localised dilation of the closed neural tube at the level of the hindlimb buds, but not terminal myelocystocele-like phenotypes at later stages, was previously observed in *Fgf3* knockout embryos (57). At the opposite extreme, a more extensive dilation of the spinal cord's central canal extending caudally from the thoracic spine has been described in *Noggin* knockout fetuses (58). Noggin is an antagonist of BMP signalling, which promotes dorsal spinal progenitor fates. Evidence of dorsoventral patterning disruption in $Noggin^{-/-}$ embryos includes ventral expansion of PAX3 (59). Another striking similarity between $Noggin^{-/-}$ and *Fgfr1*-

disrupted embryos in the current study is the preferential loss of dorsoventral patterning at the level of the hindlimb buds, although *Noggin*$^{-/-}$ embryos also have markedly smaller neural tubes making direct comparisons difficult (59). One possible explanation for this regional phenotype is interactions with adjacent mesodermal structures, which are particularly abnormal caudally in our model. This is consistent with lack of sclerotome-derived vertebral bodies below the cystic lesion of *Fgfr1*-disrupted fetuses. Sclerotome has been suggested to act both as a conduit for SHH diffusion as well as being a target tissue for its action (60) and somite-derived retinoic acid is mutually antagonistic with FGF signalling in regulating caudal neurogenesis (16). The combination of diminishing retinoic acid production by somites adjacent to the closed neural tube, and loss of repression by FGF signaling, suggests complex changes in the source, timing and intensity of neuroepithelial retinoic acid exposure in our model.

The transition from neurulation to subsequent neurogenesis continues to be explored. Premature neuronal differentiation and expansion of ventral spinal progenitor domains have been associated with open NTDs (23, 25). One model of ventral progenitor domain expansion, deletion of the mitochondrial protein *Fkbp8*, produces extensive cystic dilation of the neural tube along the entire thoracic and lumbar spine (61). Histological sections of these *Fkbp8*-deficient fetuses with ventralised neural tubes suggests thinning of the ventral spinal cord, whereas the dorsalised neural tubes of our *Fgfr1*-disrupted embryos become thinned dorsally. The mechanisms for these changes in shape are unknown, but we propose that they cause characteristic spinal dysmorphology in conditions such as terminal myelocystocele.

The multiple interacting tissues and ubiquitous roles of FGF signalling present challenges in dissecting the molecular mechanisms by which terminal myelocystocele-like lesions emerge after closure of the neural tube. Here, we characterise a new model to begin addressing these questions. Dysmorphic PNP closure, ectopic neuroepithelial cluster formation which may act as aberrant Shh sources, diminished neuroepithelial proliferation during neurulation, progressive neural tube dorsalisation, and hypoplasia of surrounding mesodermal structures, all precede trumpet-like flaring of the neural tube central canal in this model. We propose that whereas failure of neurulation causes open NTDs, abnormalities in neural patterning contribute to the spectrum of clinically recognised closed NTDs.

Materials and methods

Animal procedures

Studies were performed under the regulation of the UK Animals (Scientific Procedures) Act 1986 and the National Centre for the 3Rs' Responsibility in the Use of Animals for Medical Research (2019). C57BL/6 mice were bred in house and used as plug stock from 8 weeks of age. Mice were mated overnight, and the next morning a plug was found and considered E0.5. Alternatively, mice were mated for a few hours during the day, and the following midnight was considered E0.5. Pregnant females were sacrificed between E9.5 and E16.5.

Fgfr1$^{Fl/+}$ mice were as previously described (38). *Cdx2*$^{Cre/+}$ mice (39) were used to breed *Cdx2*^{Cre}*Fgfr1*$^{Fl/+}$ stud males. The stud males were then crossed with *Fgfr1*$^{Fl/Fl}$ females to obtain *Cdx2*^{Cre}*Fgfr1*$^{Fl/Fl}$ embryos. *Cdx2*^{Cre}*Fgfr1*$^{Fl/+}$ and Cre-negative embryos were phenotypically normal and considered littermate controls. *Rosa26-mTmG* reporter mice were as previously described (62). For lineage tracing, *Cdx2*^{Cre}*Fgfr1*$^{Fl/+}$ stud males were crossed with *Fgfr1*$^{Fl/Fl}$*mTmG* females.

To lineage-trace neuromesodermal progenitors during FGFR pharmacological inhibition, *T*$^{CreERT2/+}$ stud males (63) were crossed with *mTmG* females and tamoxifen (10 mg/mouse) was administered orally at 6 pm on E8.5 as previously validated (64). Embryos were then explanted into whole embryo culture starting at E9.5 and fixed 24 hours after the start of culture.

The RARE-hsp68LacZ reporter mice (JAX stock #008477) (65) were on a CD1 background as previously described (65).

Human embryos

One CS11 and one CS13 human embryo collected contemporaneously with this project were provided by the Human Developmental Biology Resource tissue bank (https://www.hdbr.org/), project registration number 200537. These embryos were non-destructively imaged using reflection confocal microscopy and returned to the tissue bank. Brightfield images of CD9-CS12 embryos collected by the tissue bank were also provided. These were identified from archival annotations stored by the tissue bank but were not available for further analysis.

Embryo culture

Whole mouse embryo culture was performed in neat rat serum following published protocols

(66). Pharmacological inhibitors pan-FGFRi (BGJ 398, Generon, used at a final concentration of 1 µM) or FGFR1-targeting inhibitor (PD 173074, Cambridge Bioscience, used at 1 µM) were dissolved in DMSO and added to the rat serum at the start of culture. For control conditions 0.1% DMSO was added to the rat serum. Embryos were size matched and randomized to inhibitor or vehicle groups using a coin toss.

Immunofluorescence

Embryos were dissected from their extraembryonic membranes, rinsed in ice cold PBS and fixed in 4% PFA overnight. Whole-embryo immunostaining was as previously described (5). Primary antibodies were used in 1:100 dilution and were as follows: rabbit E-cadherin (3195, Cell Signaling Technology), mouse N-cadherin (14215S, Cell Signaling Technology), rabbit pERK1/2 (#9101, Cell Signalling Technology), mouse FGFR1 (ab824, Abcam) mouse anti-RALDH2 (sc-166362, Santa Cruz),and rabbit anti pFGFR1 (Tyr 653/654, GTX133526, Stratech).

For N-cadherin staining, antigen retrieval was first performed for 25 mins at 100°C using 10 mM sodium citrate with 0.05% Tween 20, pH 6.0. For pERK staining, a methanol/acetone post-fix step was added after PFA fixation. Embryos were washed with ice cold 50:50 methanol/acetone for 30 min, followed by decreasing concentrations of methanol (10 min each) prior to blocking in 5% BSA solution in PBS with 0.1% Triton X-100. Secondary antibodies were used in 1:200 dilution and were Alexa Fluor conjugated (Thermo Fisher Scientific). Alexa Fluor 568 or 647–conjugated Phalloidin was from Thermo Fisher Scientific.

For immunostaining of paraffin sections, antigen retrieval was always performed prior to blocking in 5% BSA solution. Primary antibodies were applied overnight at 4°C (1:100-1:200 dilution). Primary antibodies were as follows: rabbit anti-SOX2 (ab97959, Abcam), rabbit anti-SOX9 (7H13L8, Thermo Fisher Scientific), mouse anti-TUJ1 (MMS-435P, BioLegend), goat anti-OLIG2 (AF2418, Novus Biologicals), rabbit anti-SHH (C9C5, Cell Signalling Technology), mouse PAX3 (Pax3-c, DSHB), rabbit anti-PAX6 (901301, BioLegend), goat anti-FOXA2 (AF2400, R&D Systems), and mouse anti-HuC/D (16A11, Thermo Fisher). Sections were washed, incubated with the secondary antibodies above (1:500 dilution) and counterstained with DAPI for 2 h at room temperature.

Confocal microscopy and image analysis

Images were captured on a Zeiss Examiner LSM 880 confocal using 10 x/NA 0.5 or 20 x/NA 1.0 Plan Apochromat water immersion objectives. Images were processed with Zen 2.3 software and visualized as maximum projections in Fiji (67). Inset in Figure 1F was obtained with AiryFast scanning mode using the 20x/NA 1.0 water immersion objective. Reflection images of CS11 and CS13 human embryos were captured at 633 nm wavelength using a 10x/NA 0.5 water immersion objective. The z stacks were 3D rotated and visualised as maximum projections. Sections were captured with AiryFast scanning mode using the 10X/NA 0.5 dipping objective. Salt and pepper noise was removed when appropriate using the de-speckle or 'remove outliers' function in Fiji. 'Surface subtraction' was used to extract surface signal in wholemount images using an in-house macro as previously described (6). This macro is available courtesy of Dr. Dale Moulding on GitHub (https://github.com/DaleMoulding/Fiji-Macros).

For morphometric analysis, PNP length and width were calculated by annotating the PNP rim and then measuring the major and minor axis using the fit ellipse function in Fiji. Neural fold elevation was measured in optical reslices of confocal Z-stacks. Distances between the limb buds and the caudal end of the embryos were measured in stereoscope images using the segmented line tool in Fiji. Floor plate area was measured using the polygon tool and is expressed as percentage of total neural tube area.

Histology and X-gal staining

Following overnight fixation in 4% PFA, E11.5 embryos were dehydrated with increasing concentrations of ethanol (20 min each). They were then moved to 100% histoclear for 20 min at room temperature, washed twice with 50:50 histoclear/paraffin mix for 10 min at 65°C and then embedded in 100% paraffin. Paraffin was replaced three times to ensure removal of histoclear. Sections were made at 10 µm thickness. The protocol was similar for E14.5 fetuses except for longer dehydration steps (40 min each), followed by overnight storage in 100% ethanol. In this case, histoclear was added for 40 min at room temperature. Sections were either antibody stained (see immunofluorescence) or stained with hematoxylin and eosin. For bone staining, P1 pups were fixed overnight in 100% ethanol followed by three days in 100% acetone. They were then stained with Dawson staining solution overnight at 37°C, washed and cleared with 1% KOH at 37^{o}C. Slower clearing was achieved with 10% glycerol in 1% KOH at RT. For Xgal staining, embryos were removed from culture and fixed in 2% PFA for 10 min,

rinsed in 2 mM $MgCl_2$ in PBS and incubated in staining solution: 1× PBS, 20mM K3Fe(CN)6, 20mM K4Fe(CN)6-3H2O, 2mM MgCl2, 0.01% sodium deoxycholate, 0.02% NP-40 with X-gal (1 mg/ml final concentration) as a 1:50 addition at 37°C for 3 hours.

In situ hybridization

In situ hybridisation of whole E10.5 embryos was performed essentially as previously described (68) using a cDNA probe for *Fgf8* ((69) *variant 4,* insert 800 bp) cloned into a pBluescript SK(+) vector. Sense and anti-sense riboprobes were generated using a digoxygenin RNA labelling kit and T3/T7 RNA polymerases (Roche). Images are representative of at least 3 embryos per condition.

Statistical analysis

Statistical analysis was performed in OriginPro 2017 (Origin Labs). Individual embryos were the unit of measure. Comparison of two groups was by Student's *t* test. Proportions were compared using Fisher's exact tests. Comparisons of slopes were based on Pearson's correlation. Graphs were made in OriginPro 2017 and are shown as dot-plots or scatter plots. Analysis of Closure 5 presence was carried out blinded to genotype/treatment group, although marked PNP dysmorphology could not be masked in these analyses.

Acknowledgements

This study was supported by the Wellcome Trust (211112/Z/18/Z and 211112/Z/18/A, both to GLG). The NIHR Great Ormond Street Hospital Biomedical Research Centre (NIHR GOSH BRC) supports research infrastructure at the UCL GOS Institute of Child Health. The views expressed are those of the authors and not necessarily those of the NHS, the NIHR or the Department of Health. EM is funded by Marie Slodowska-Curie Actions Project 101067028. The human embryonic material was provided by the joint MRC/Wellcome Trust (grant # MR/R006237/1) Human Developmental Biology Resource (www.hdbr.org). Use of *Fgfr1*-floxed alleles was with permission of their creator, Prof Chu-Xia Deng, and we are grateful to Dr Emma

Rawlins for providing these mice. We thank Mr Dominic Thompson for discussions of terminal myelocystocele phenotypes.

Conflicts of interest

The authors declare they have no relevant conflicts of interest.

References

1. E. Nikolopoulou, G. L. Galea, A. Rolo, N. D. Greene, A. J. Copp, Neural tube closure: cellular, molecular and biomechanical mechanisms. *Development* **144**, 552-566 (2017).
2. M. I. Van Allen, D. K. Kalousek, G. F. Chernoff, D. Juriloff, M. Harris, B. C. McGillivray, S. L. Yong, S. Langlois, P. M. MacLeod, D. Chitayat, et al., Evidence for multi-site closure of the neural tube in humans. *Am J Med Genet* **47**, 723-743 (1993).
3. M. L. Martinez-Frias, M. Urioste, E. Bermejo, A. Sanchis, E. Rodriguez-Pinilla, Epidemiological analysis of multi-site closure failure of neural tube in humans. *Am J Med Genet* **66**, 64-68 (1996).
4. A. J. Copp, N. D. Greene, Genetics and development of neural tube defects. *J Pathol* **220**, 217-230 (2010).
5. G. L. Galea, Y. J. Cho, G. Galea, M. A. Mole, A. Rolo, D. Savery, D. Moulding, L. H. Culshaw, E. Nikolopoulou, N. D. E. Greene, A. J. Copp, Biomechanical coupling facilitates spinal neural tube closure in mouse embryos. *Proc Natl Acad Sci U S A* **114**, E5177-E5186 (2017).
6. G. L. Galea, O. Nychyk, M. A. Mole, D. Moulding, D. Savery, E. Nikolopoulou, D. J. Henderson, N. D. E. Greene, A. J. Copp, Vangl2 disruption alters the biomechanics of late spinal neurulation leading to spina bifida in mouse embryos. *Dis Model Mech* **11** (2018).
7. J. Yang, J. Y. Lee, K. H. Kim, H. J. Yang, K. C. Wang, Disorders of Secondary Neurulation: Suggestion of a New Classification According to Pathoembryogenesis. *Adv Tech Stand Neurosurg* **45**, 285-315 (2022).
8. A. J. Copp, N. D. Greene, Neural tube defects--disorders of neurulation and related embryonic processes. *Wiley Interdiscip Rev Dev Biol* **2**, 213-227 (2013).
9. J. Y. Lee, K. H. Kim, K. C. Wang, Terminal Myelocystocele : Pathoembryogenesis and Clinical Features. *J Korean Neurosurg Soc* **63**, 321-326 (2020).

10. D. Pang, J. Zovickian, J. Y. Lee, G. S. Moes, K. C. Wang, Terminal myelocystocele: surgical observations and theory of embryogenesis. *Neurosurgery* **70**, 1383-1404; discussion 1404-1385 (2012).
11. A. S. Shum, L. S. Tang, A. J. Copp, H. Roelink, Lack of motor neuron differentiation is an intrinsic property of the mouse secondary neural tube. *Dev Dyn* **239**, 3192-3203 (2010).
12. E. Agius, C. Soukkarieh, C. Danesin, P. Kan, H. Takebayashi, C. Soula, P. Cochard, Converse control of oligodendrocyte and astrocyte lineage development by Sonic hedgehog in the chick spinal cord. *Dev Biol* **270**, 308-321 (2004).
13. Y. Nishi, X. Zhang, J. Jeong, K. A. Peterson, A. Vedenko, M. L. Bulyk, W. A. Hide, A. P. McMahon, A direct fate exclusion mechanism by Sonic hedgehog-regulated transcriptional repressors. *Development* **142**, 3286-3293 (2015).
14. E. Dessaud, L. L. Yang, K. Hill, B. Cox, F. Ulloa, A. Ribeiro, A. Mynett, B. G. Novitch, J. Briscoe, Interpretation of the sonic hedgehog morphogen gradient by a temporal adaptation mechanism. *Nature* **450**, 717-720 (2007).
15. N. Balaskas, A. Ribeiro, J. Panovska, E. Dessaud, N. Sasai, K. M. Page, J. Briscoe, V. Ribes, Gene regulatory logic for reading the Sonic Hedgehog signaling gradient in the vertebrate neural tube. *Cell* **148**, 273-284 (2012).
16. R. Diez del Corral, D. N. Breitkreuz, K. G. Storey, Onset of neuronal differentiation is regulated by paraxial mesoderm and requires attenuation of FGF signalling. *Development* **129**, 1681-1691 (2002).
17. V. Lobjois, B. Benazeraf, N. Bertrand, F. Medevielle, F. Pituello, Specific regulation of cyclins D1 and D2 by FGF and Shh signaling coordinates cell cycle progression, patterning, and differentiation during early steps of spinal cord development. *Dev Biol* **273**, 195-209 (2004).
18. R. Diez Del Corral, A. V. Morales, The Multiple Roles of FGF Signaling in the Developing Spinal Cord. *Front Cell Dev Biol* **5**, 58 (2017).
19. V. Ribes, I. Le Roux, M. Rhinn, B. Schuhbaur, P. Dolle, Early mouse caudal development relies on crosstalk between retinoic acid, Shh and Fgf signalling pathways. *Development* **136**, 665-676 (2009).
20. B. G. Novitch, H. Wichterle, T. M. Jessell, S. Sockanathan, A requirement for retinoic acid-mediated transcriptional activation in ventral neural patterning and motor neuron specification. *Neuron* **40**, 81-95 (2003).

21. R. Diez del Corral, I. Olivera-Martinez, A. Goriely, E. Gale, M. Maden, K. Storey, Opposing FGF and retinoid pathways control ventral neural pattern, neuronal differentiation, and segmentation during body axis extension. *Neuron* **40**, 65-79 (2003).
22. N. Molotkova, A. Molotkov, I. O. Sirbu, G. Duester, Requirement of mesodermal retinoic acid generated by Raldh2 for posterior neural transformation. *Mech Dev* **122**, 145-155 (2005).
23. S. Sudiwala, A. Palmer, V. Massa, A. J. Burns, L. P. E. Dunlevy, S. C. P. de Castro, D. Savery, K. Y. Leung, A. J. Copp, N. D. E. Greene, Cellular mechanisms underlying Pax3-related neural tube defects and their prevention by folic acid. *Dis Model Mech* **12** (2019).
24. D. J. Epstein, M. Vekemans, P. Gros, Splotch (Sp2H), a mutation affecting development of the mouse neural tube, shows a deletion within the paired homeodomain of Pax-3. *Cell* **67**, 767-774 (1991).
25. V. L. Patterson, C. Damrau, A. Paudyal, B. Reeve, D. T. Grimes, M. E. Stewart, D. J. Williams, P. Siggers, A. Greenfield, J. N. Murdoch, Mouse hitchhiker mutants have spina bifida, dorso-ventral patterning defects and polydactyly: identification of Tulp3 as a novel negative regulator of the Sonic hedgehog pathway. *Hum Mol Genet* **18**, 1719-1739 (2009).
26. J. Qin, Y. Lin, R. X. Norman, H. W. Ko, J. T. Eggenschwiler, Intraflagellar transport protein 122 antagonizes Sonic Hedgehog signaling and controls ciliary localization of pathway components. *Proc Natl Acad Sci U S A* **108**, 1456-1461 (2011).
27. T. P. Yamaguchi, K. Harpal, M. Henkemeyer, J. Rossant, fgfr-1 is required for embryonic growth and mesodermal patterning during mouse gastrulation. *Genes Dev* **8**, 3032-3044 (1994).
28. F. Gofflot, M. Hall, G. M. Morriss-Kay, Genetic patterning of the developing mouse tail at the time of posterior neuropore closure. *Dev Dyn* **210**, 431-445 (1997).
29. H. J. Yang, D. H. Lee, Y. J. Lee, J. G. Chi, J. Y. Lee, J. H. Phi, S. K. Kim, B. K. Cho, K. C. Wang, Secondary neurulation of human embryos: morphological changes and the expression of neuronal antigens. *Childs Nerv Syst* **30**, 73-82 (2014).
30. A. Goldbeter, D. Gonze, O. Pourquie, Sharp developmental thresholds defined through bistability by antagonistic gradients of retinoic acid and FGF signaling. *Dev Dyn* **236**, 1495-1508 (2007).
31. J. S. Colvin, B. A. Bohne, G. W. Harding, D. G. McEwen, D. M. Ornitz, Skeletal overgrowth and deafness in mice lacking fibroblast growth factor receptor 3. *Nat Genet* **12**, 390-397 (1996).

32. X. Xu, M. Weinstein, C. Li, M. Naski, R. I. Cohen, D. M. Ornitz, P. Leder, C. Deng, Fibroblast growth factor receptor 2 (FGFR2)-mediated reciprocal regulation loop between FGF8 and FGF10 is essential for limb induction. *Development* **125**, 753-765 (1998).

33. M. B. Wahl, C. Deng, M. Lewandoski, O. Pourquie, FGF signaling acts upstream of the NOTCH and WNT signaling pathways to control segmentation clock oscillations in mouse somitogenesis. *Development* **134**, 4033-4041 (2007).

34. C. Deng, M. Bedford, C. Li, X. Xu, X. Yang, J. Dunmore, P. Leder, Fibroblast growth factor receptor-1 (FGFR-1) is essential for normal neural tube and limb development. *Dev Biol* **185**, 42-54 (1997).

35. M. Mohammadi, S. Froum, J. M. Hamby, M. C. Schroeder, R. L. Panek, G. H. Lu, A. V. Eliseenkova, D. Green, J. Schlessinger, S. R. Hubbard, Crystal structure of an angiogenesis inhibitor bound to the FGF receptor tyrosine kinase domain. *EMBO J* **17**, 5896-5904 (1998).

36. J. Szymczyk, M. Sochacka, P. Chudy, L. Opalinski, J. Otlewski, M. Zakrzewska, FGF1 protects FGFR1-overexpressing cancer cells against drugs targeting tubulin polymerization by activating AKT via two independent mechanisms. *Front Oncol* **12**, 1011762 (2022).

37. J. R. Brewer, A. Molotkov, P. Mazot, R. V. Hoch, P. Soriano, Fgfr1 regulates development through the combinatorial use of signaling proteins. *Genes Dev* **29**, 1863-1874 (2015).

38. X. Xu, W. Qiao, C. Li, C. X. Deng, Generation of Fgfr1 conditional knockout mice. *Genesis* **32**, 85-86 (2002).

39. T. Hinoi, A. Akyol, B. K. Theisen, D. O. Ferguson, J. K. Greenson, B. O. Williams, K. R. Cho, E. R. Fearon, Mouse model of colonic adenoma-carcinoma progression based on somatic Apc inactivation. *Cancer Res* **67**, 9721-9730 (2007).

40. H. W. van Straaten, A. J. Copp, Curly tail: a 50-year history of the mouse spina bifida model. *Anat Embryol (Berl)* **203**, 225-237 (2001).

41. N. D. Greene, A. J. Copp, Mouse models of neural tube defects: investigating preventive mechanisms. *Am J Med Genet C Semin Med Genet* **135C**, 31-41 (2005).

42. M. Meuli, C. Meuli-Simmen, G. M. Hutchins, C. D. Yingling, K. M. Hoffman, M. R. Harrison, N. S. Adzick, In utero surgery rescues neurological function at birth in sheep with spina bifida. *Nat Med* **1**, 342-347 (1995).

43. H. Goto, S. C. Kimmey, R. H. Row, D. Q. Matus, B. L. Martin, FGF and canonical Wnt signaling cooperate to induce paraxial mesoderm from tailbud neuromesodermal progenitors through regulation of a two-step epithelial to mesenchymal transition. *Development* **144**, 1412-1424 (2017).

44. D. A. Turner, P. C. Hayward, P. Baillie-Johnson, P. Rue, R. Broome, F. Faunes, A. Martinez Arias, Wnt/beta-catenin and FGF signalling direct the specification and maintenance of a neuromesodermal axial progenitor in ensembles of mouse embryonic stem cells. *Development* **141**, 4243-4253 (2014).

45. R. Sambasivan, B. Steventon, Neuromesodermal Progenitors: A Basis for Robust Axial Patterning in Development and Evolution. *Front Cell Dev Biol* **8**, 607516 (2020).

46. I. Olivera-Martinez, H. Harada, P. A. Halley, K. G. Storey, Loss of FGF-dependent mesoderm identity and rise of endogenous retinoid signalling determine cessation of body axis elongation. *PLoS Biol* **10**, e1001415 (2012).

47. C. A. Pearson, K. Ohyama, L. Manning, S. Aghamohammadzadeh, H. Sang, M. Placzek, FGF-dependent midline-derived progenitor cells in hypothalamic infundibular development. *Development* **138**, 2613-2624 (2011).

48. M. Murphy, J. Drago, P. F. Bartlett, Fibroblast growth factor stimulates the proliferation and differentiation of neural precursor cells in vitro. *J Neurosci Res* **25**, 463-475 (1990).

49. G. Minowada, L. A. Jarvis, C. L. Chi, A. Neubuser, X. Sun, N. Hacohen, M. A. Krasnow, G. R. Martin, Vertebrate Sprouty genes are induced by FGF signaling and can cause chondrodysplasia when overexpressed. *Development* **126**, 4465-4475 (1999).

50. J. Dubrulle, M. J. McGrew, O. Pourquie, FGF signaling controls somite boundary position and regulates segmentation clock control of spatiotemporal Hox gene activation. *Cell* **106**, 219-232 (2001).

51. J. M. Verheyden, M. Lewandoski, C. Deng, B. D. Harfe, X. Sun, Conditional inactivation of Fgfr1 in mouse defines its role in limb bud establishment, outgrowth and digit patterning. *Development* **132**, 4235-4245 (2005).

52. D. P. Poladia, K. Kish, B. Kutay, D. Hains, H. Kegg, H. Zhao, C. M. Bates, Role of fibroblast growth factor receptors 1 and 2 in the metanephric mesenchyme. *Dev Biol* **291**, 325-339 (2006).

53. X. Xu, C. Li, K. Takahashi, H. C. Slavkin, L. Shum, C. X. Deng, Murine fibroblast growth factor receptor 1alpha isoforms mediate node regression and are essential for posterior mesoderm development. *Dev Biol* **208**, 293-306 (1999).

54. S. G. Gong, Isoforms of receptors of fibroblast growth factors. *J Cell Physiol* **229**, 1887-1895 (2014).
55. A. Rolo, G. L. Galea, D. Savery, N. D. E. Greene, A. J. Copp, Novel mouse model of encephalocele: post-neurulation origin and relationship to open neural tube defects. *Dis Model Mech* **12** (2019).
56. R. V. Hoch, P. Soriano, Context-specific requirements for Fgfr1 signaling through Frs2 and Frs3 during mouse development. *Development* **133**, 663-673 (2006).
57. M. J. Anderson, T. Schimmang, M. Lewandoski, An FGF3-BMP Signaling Axis Regulates Caudal Neural Tube Closure, Neural Crest Specification and Anterior-Posterior Axis Extension. *PLoS Genet* **12**, e1006018 (2016).
58. R. W. Stottmann, M. Berrong, K. Matta, M. Choi, J. Klingensmith, The BMP antagonist Noggin promotes cranial and spinal neurulation by distinct mechanisms. *Dev Biol* **295**, 647-663 (2006).
59. J. A. McMahon, S. Takada, L. B. Zimmerman, C. M. Fan, R. M. Harland, A. P. McMahon, Noggin-mediated antagonism of BMP signaling is required for growth and patterning of the neural tube and somite. *Genes Dev* **12**, 1438-1452 (1998).
60. N. Kahane, C. Kalcheim, Neural tube development depends on notochord-derived sonic hedgehog released into the sclerotome. *Development* **147** (2020).
61. R. L. Wong, B. J. Wlodarczyk, K. S. Min, M. L. Scott, S. Kartiko, W. Yu, M. Y. Merriweather, P. Vogel, B. P. Zambrowicz, R. H. Finnell, Mouse Fkbp8 activity is required to inhibit cell death and establish dorso-ventral patterning in the posterior neural tube. *Hum Mol Genet* **17**, 587-601 (2008).
62. M. D. Muzumdar, B. Tasic, K. Miyamichi, L. Li, L. Luo, A global double-fluorescent Cre reporter mouse. *Genesis* **45**, 593-605 (2007).
63. M. J. Anderson, L. A. Naiche, C. P. Wilson, C. Elder, D. A. Swing, M. Lewandoski, TCreERT2, a transgenic mouse line for temporal control of Cre-mediated recombination in lineages emerging from the primitive streak or tail bud. *PLoS One* **8**, e62479 (2013).
64. D. Savery, E. Maniou, L. H. Culshaw, N. D. E. Greene, A. J. Copp, G. L. Galea, Refinement of inducible gene deletion in embryos of pregnant mice. *Birth Defects Res* **112**, 196-204 (2020).
65. J. Rossant, R. Zirngibl, D. Cado, M. Shago, V. Giguere, Expression of a retinoic acid response element-hsplacZ transgene defines specific domains of transcriptional activity during mouse embryogenesis. *Genes Dev* **5**, 1333-1344 (1991).
66. S. E. Pryor, V. Massa, D. Savery, N. D. Greene, A. J. Copp, Convergent extension analysis in mouse whole embryo culture. *Methods Mol Biol* **839**, 133-146 (2012).

67. J. Schindelin, I. Arganda-Carreras, E. Frise, V. Kaynig, M. Longair, T. Pietzsch, S. Preibisch, C. Rueden, S. Saalfeld, B. Schmid, J. Y. Tinevez, D. J. White, V. Hartenstein, K. Eliceiri, P. Tomancak, A. Cardona, Fiji: an open-source platform for biological-image analysis. *Nat Methods* **9**, 676-682 (2012).

68. P. Ybot-Gonzalez, A. J. Copp, N. D. Greene, Expression pattern of glypican-4 suggests multiple roles during mouse development. *Dev Dyn* **233**, 1013-1017 (2005).

69. P. H. Crossley, G. R. Martin, The mouse Fgf8 gene encodes a family of polypeptides and is expressed in regions that direct outgrowth and patterning in the developing embryo. *Development* **121**, 439-451 (1995).

Figures

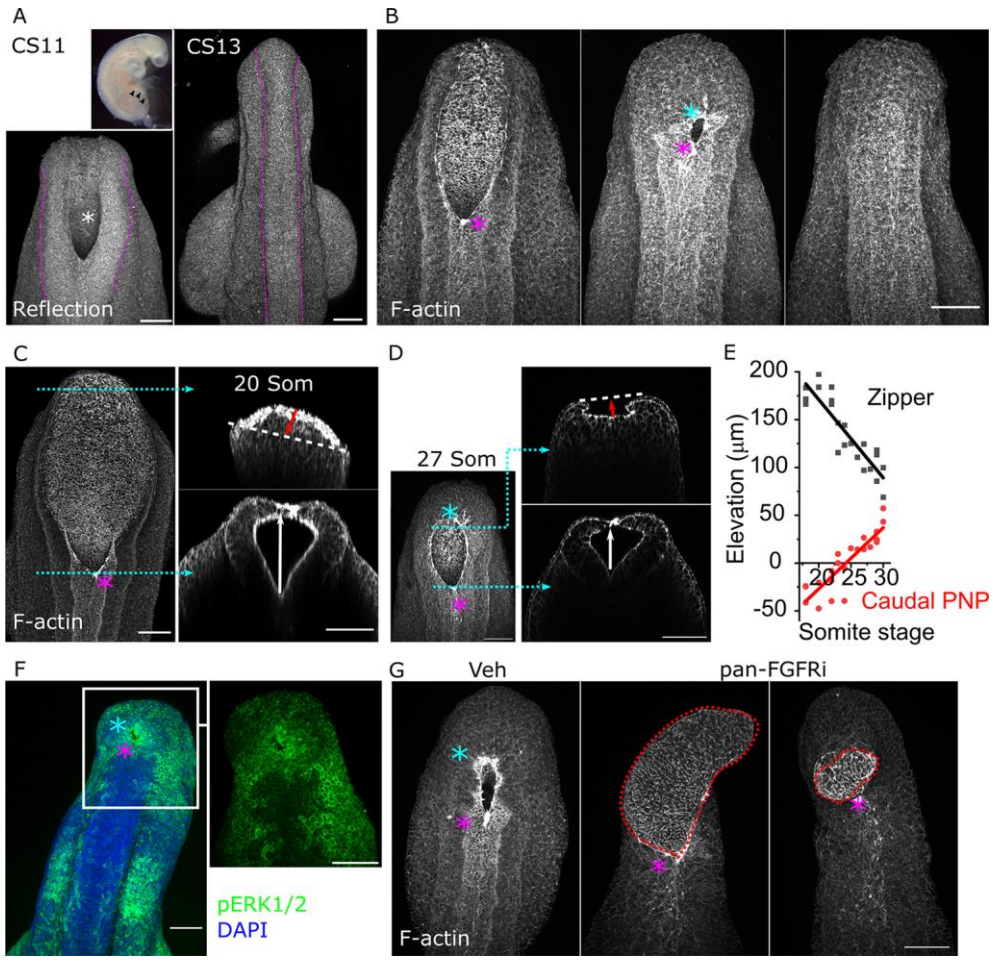

Fig. 1. FGF-dependent elevation of the distal neural folds forms Closure 5.

A. Reflection confocal images of the PNP of a CS11 (* and black arrowheads in insert) and closed neural tube of a CS13 human embryo. Dashed magenta lines indicate the borders of the neuroepithelium. Scale bars = 50 µm.

B. Representative confocal images of phalloidin-stained mouse PNPs at sequential stages of closure (E9.5-E10.5) illustrating the formation of Closure 5 and completion of closure. Scale bar = 100 µm.

C. Confocal image of a phalloidin-stained PNP from a 20-somite stage mouse embryo showing optical cross-sections at the level of the zippering point and at 90% of the PNP's length from

the proximal end. The white arrow indicates zippering point elevation, red arrow indicates eversion of the caudal neural folds relative to the apical surface of the neuroepithelium.

D. Equivalent to C showing a 27-somite stage mouse embryo PNP indicating elevation of the caudal neural folds.
E. Quantification of elevation at the zippering point and caudal neural folds (90% of the PNP's length) in mouse embryos at the indicated somite stages.
F. Wholemount-stained confocal image of a 29 somite-stage mouse PNP showing pERK1/2 immunolocalization. Scale bar = 100 µm.
G. Confocal images of a vehicle-treated and two pan-FGFR inhibitor-treated mouse embryos after 24 hours of whole embryo culture. Dashed red lines indicate the abnormal neuroepithelium which protrudes out of the PNP in inhibitor-treated embryos. Scale bar = 100 µm.

Magenta asterisks indicates the rostral zippering point, cyan asterisks indicate Closure 5.

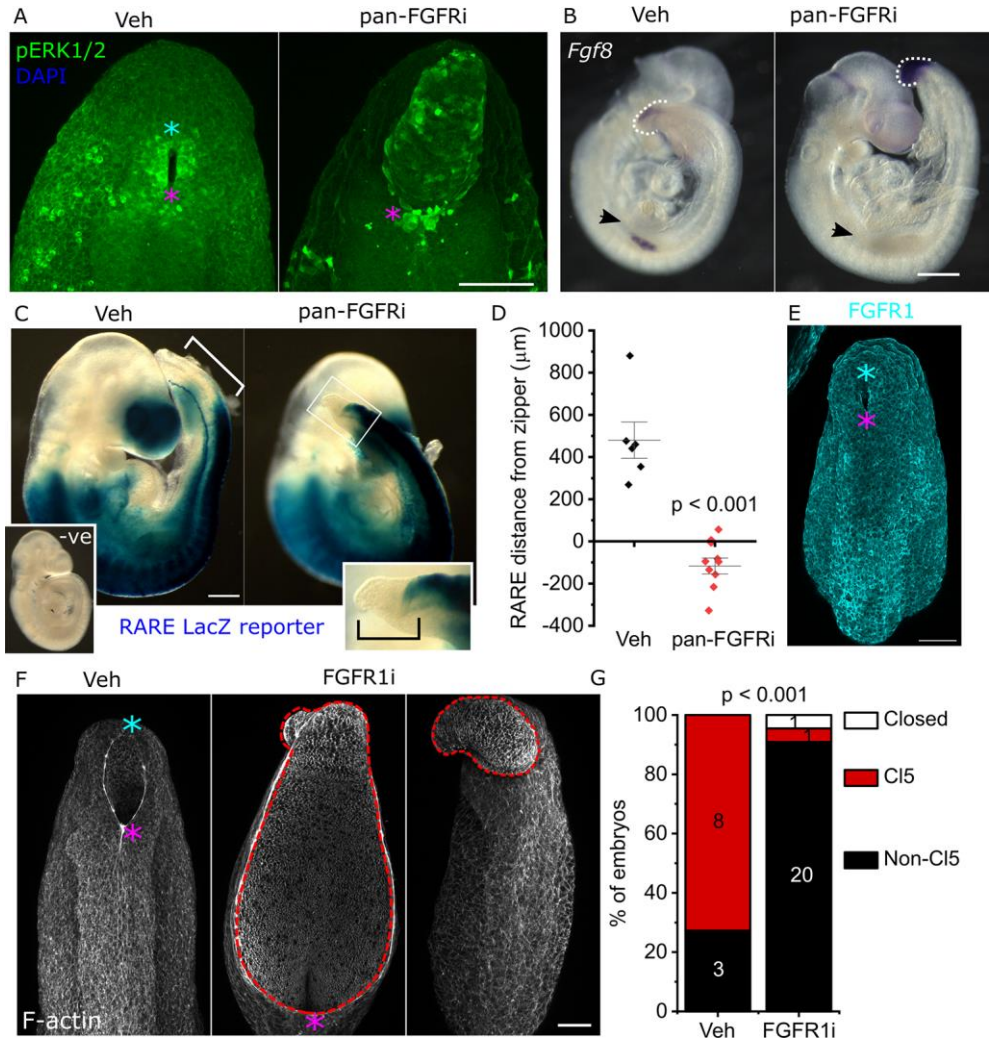

Fig. 2. FGF signalling is required for timely PNP closure.

A. Wholemount-stained confocal images showing pERK1/2 immunolocalization in a vehicle and pan-FGFRi-treated embryos after 24 hours of whole embryo culture. Note persistence of pERK-bright cells around the PNP rim in the pan-FGFRi-treated embryo. Scale bar = 100 µm.

B. Wholemount *Fgf8* in situ hybridisation in vehicle- and pan-FGFRi-treated embryos after 8 hours of whole embryo culture. Dashed white lines indicate the end of the tailbud, arrows indicate the forelimb buds. Scale bar = 500 µm.

C. Brightfield images showing RARE-mediated LacZ expression domain in vehicle and pan-FGFRi-treated embryos after 24 hours of whole embryos culture. An equivalently processed negative (-ve) control embryo lacking LacZ is also shown. The double-headed white arrow

indicates the distance between the RARE domain and the zippering point. The black bracket in the inset indicates that the RARE domain does not extend to the end of the PNP in pan-FGFRi-treated embryos. Scale bar = 350 µm.

D. Quantification of RARE domain distance to the end of zippering point in vehicle and pan-FGFRi-treated embryos after 24 hours of whole embryo culture. Point represent individual embryos, p value by T-test.

E. Wholemount immunolocalization of Fgfr1 in a 28-somite stage embryo. Scale bar = 100 µm.

F. Confocal images of embryos treated with vehicle or a second, Fgfr1-targeting antagonist after 24 hours of whole embryo culture. Dashed red lines outline the abnormal neuroepithelium in inhibitor-treated embryos. Scale bar = 100 µm.

G. Quantification of the proportion of embryos with closed PNPs, open PNPs with Closure 5 morphology (caudally narrowed PNP with elevated caudal neural folds which meet dorsally) or open PNPs without Closure 5 in vehicle and FGFR1-targeting inhibitor-treated embryos after 24 hours of whole embryo culture. Numbers indicate the number of embryos observed in each category.

Magenta asterisks indicates the rostral zippering point, cyan asterisks indicate Closure 5.

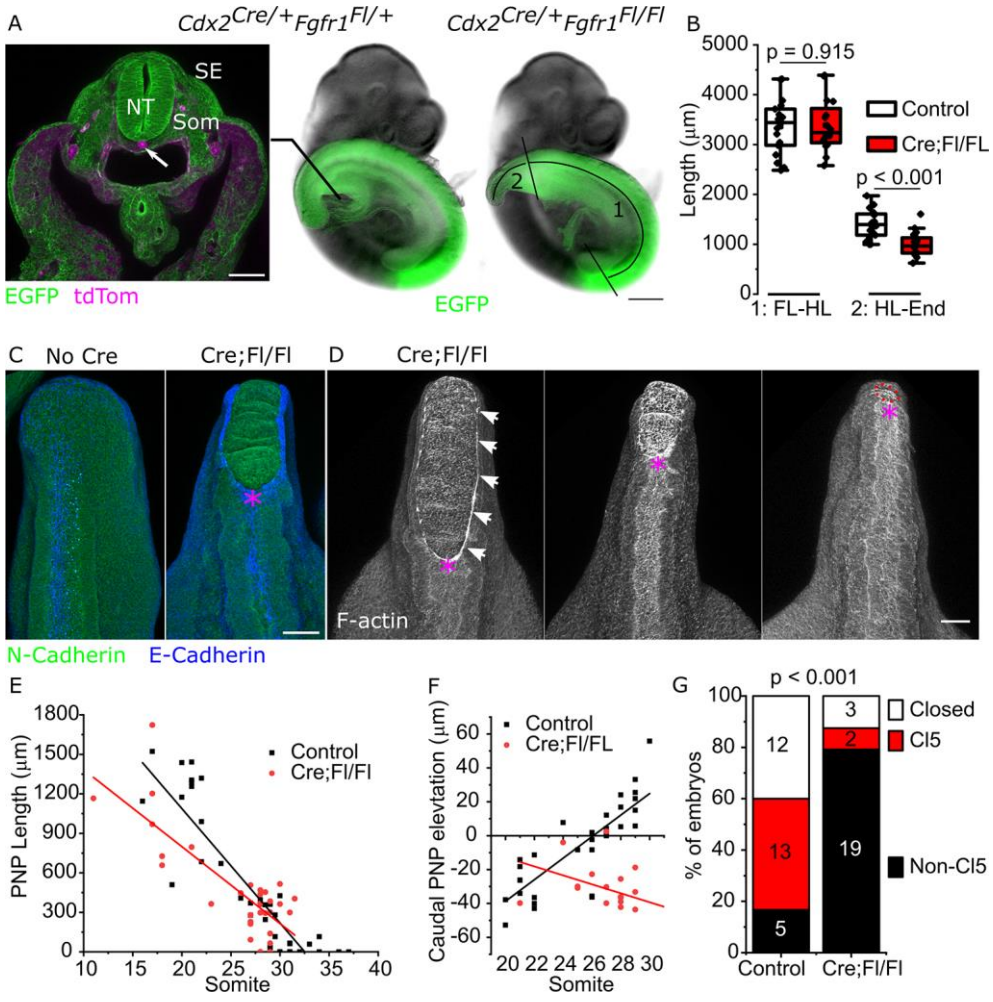

Fig. 3. Caudal genetic deletion of Fgfr1 impairs Closure 5 formation and progression of PNP closure without diminishing embryo viability.

A. E10.5 embryos showing the *Cdx2*^{Cre}-recombination domain lineage traced using mTmG (EGFP) as a confocal-imaged cross-section and brightfield images. NT neural tube, Som somite, SE surface ectoderm. 1: forelimb (FL) to hindlimb (HL) distance, 2: hindlimb to tail end distances quantified in B. Scale bars = 100 µm (confocal) and 400 µm (brightfield).
B. Quantifications of FL-HL and HL-tail end lengths in 28-31 somite stage embryos.
C. Confocal images of wholemount immunofluorescently stained embryos showing E- and N-cadherin localization in E10.5 embryos with no Cre and Cre;Fl/Fl littermate.
D. Wholemount images of three phalloidin-stained Cre;Fl/Fl embryos collected at E10.5 suggesting continued PNP closure. Scale bars = 100 µm.

E. Quantification of PNP length versus somite stage in embryos collected at E9.5-E10.5.
F. Quantification of caudal neural fold elevation (90% of PNP length) in in embryos collected at E9.5-E10.5.
G. Quantification of the proportion of embryos collected at E10.5 with closed PNPs, open PNPs with Closure 5 morphology or open PNPs without Closure 5. Numbers indicate the number of embryos observed in each category.

Magenta asterisks indicates the rostral zippering point, cyan asterisks indicate Closure 5.

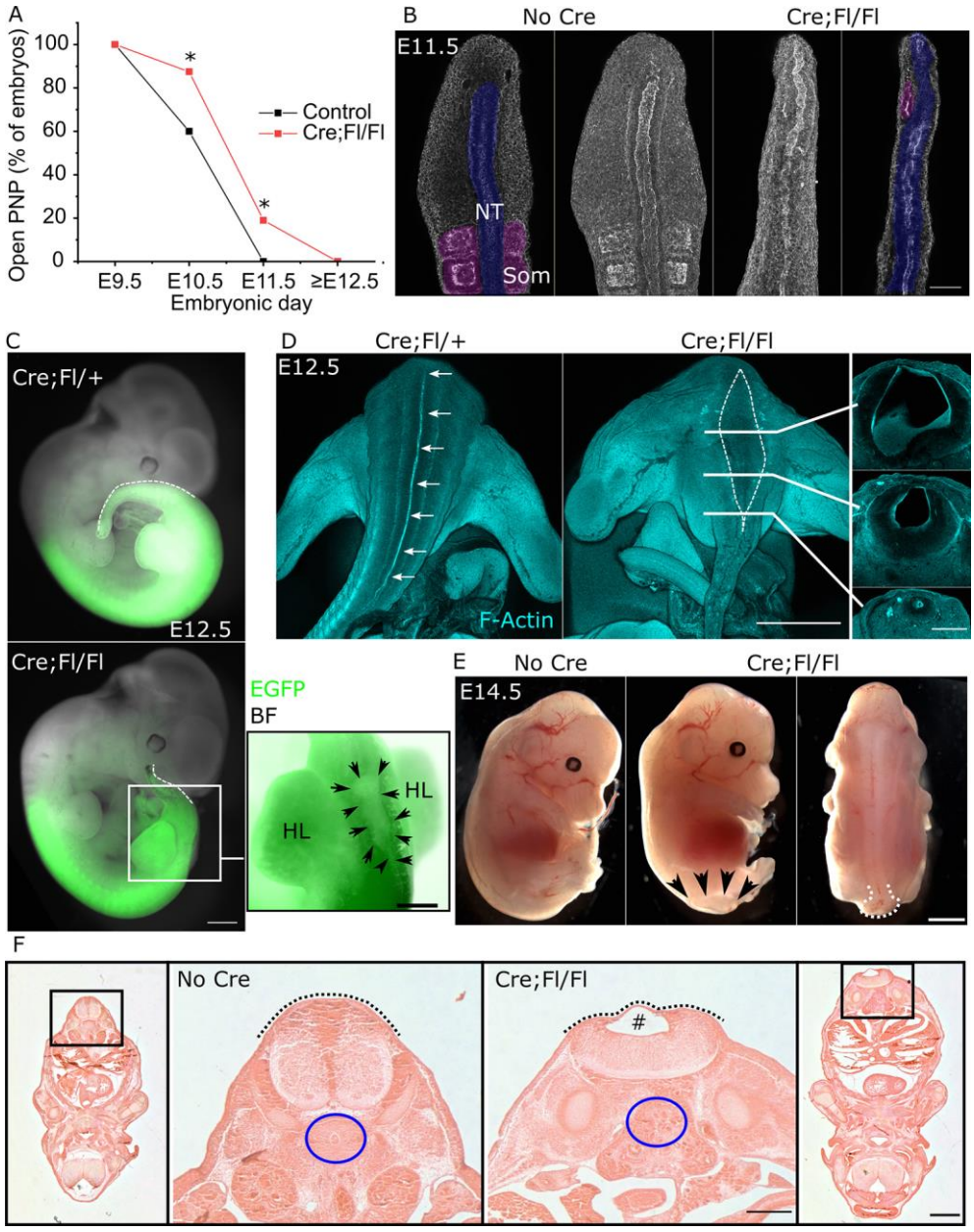

Fig. 4. Regional deletion of Fgfr1 causes delayed PNP closure and localized terminal dilation of the neural tube central canal.

A. Proportion of control and Cre;Fl/Fl embryos collected with open spinal neural tubes at the days indicated. * $p < 0.05$ by Fisher's exact test.

B. Wholemount maximum projections flanked by optical cross-sections through the caudal end of a control and Cre;Fl/Fl littermate showing the neural tube (NT) and adjacent somites (Som). Scale bar = 100 μm.

C. Brightfield images showing the *Cdx2*^{Cre} recombination domain (green, EGFP) at E12.5 in a Cre;Fl/+ control and Cre;Fl/Fl littermate. The dashed white line indicates the dorsal tail border. Black arrowheads in the inset demarcate the cystic neural tube lumen. Scale bars = 300 µm (whole embryo) and 150 µm (inset). BF brightfield.

D. Wholemount phalloidin stained embryos showing the continuous, narrow neural tube lumen in the control (arrows) in the control and dilated lumen (dashed white line) in the Cre;Fl/Fl embryo. Solid lines indicate the positions of sections taken through the same Cre;Fl/Fl embryo. Scale bars = 1 mm (wholemount) and 250 µm (section).

E. Brightfield images of a control and littermate Cre;Fl/Fl fetuses collected at E14.5. Black arrows indicate the extent of the spinal lesion in the Cre;Fl/Fl embryo and the white dashed line indicates its sac-like dilation. Scale bar = 750 µm.

F. Hematoxylin and eosin-stained sections through control and Cre;Fl/Fl littermates collected at E14.5. Dashed black lines indicate continuous skin covering, # indicates cystic dilation of the spinal cord lumen, blue circles indicate the ventral vertebral body in the control which is absent in the Cre;F/Fl. Scale bars = 300 µm (low-mag) and 100 µm (high-mag).

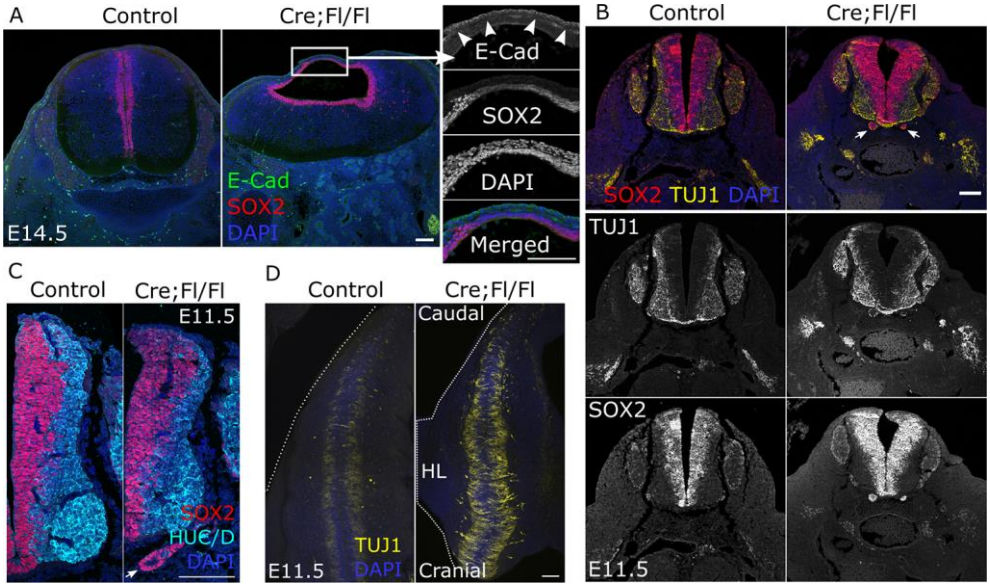

Fig. 5. Neuroepithelial commitment to post-mitotic neurons is not diminished by loss of *Fgfr1*.

A. Immunofluorescent localization of the neuroepithelial marker SOX2 and epidermal marker E-cadherin (arrowheads in insert) through the distal spinal cord of a control and Cre;Fl/Fl fetus. Scale bars = 100 µm.

B-C. Progenitor (SOX2) and committed neuron (B = TUJ1, C = HUC/D) immunofluorescence of sections through the low-lumbar spinal cord of a control and Cre;Fl/Fl embryo collected at E11.5. Note ectopic clusters of SOX2-positive cells below the neural tube of the Cre;Fl/Fl embryo (white arrows, described below). Scale bar = 100 µm.

D. Wholemount confocal images showing TUJ1 immunolocalization in the dorsal aspect of a control and littermate Cre;Fl/Fl embryo collected at E11.5 and imaged equivalently. Dashed white lines indicate the body outline, HL hindlimb. Scale bar = 100 µm.

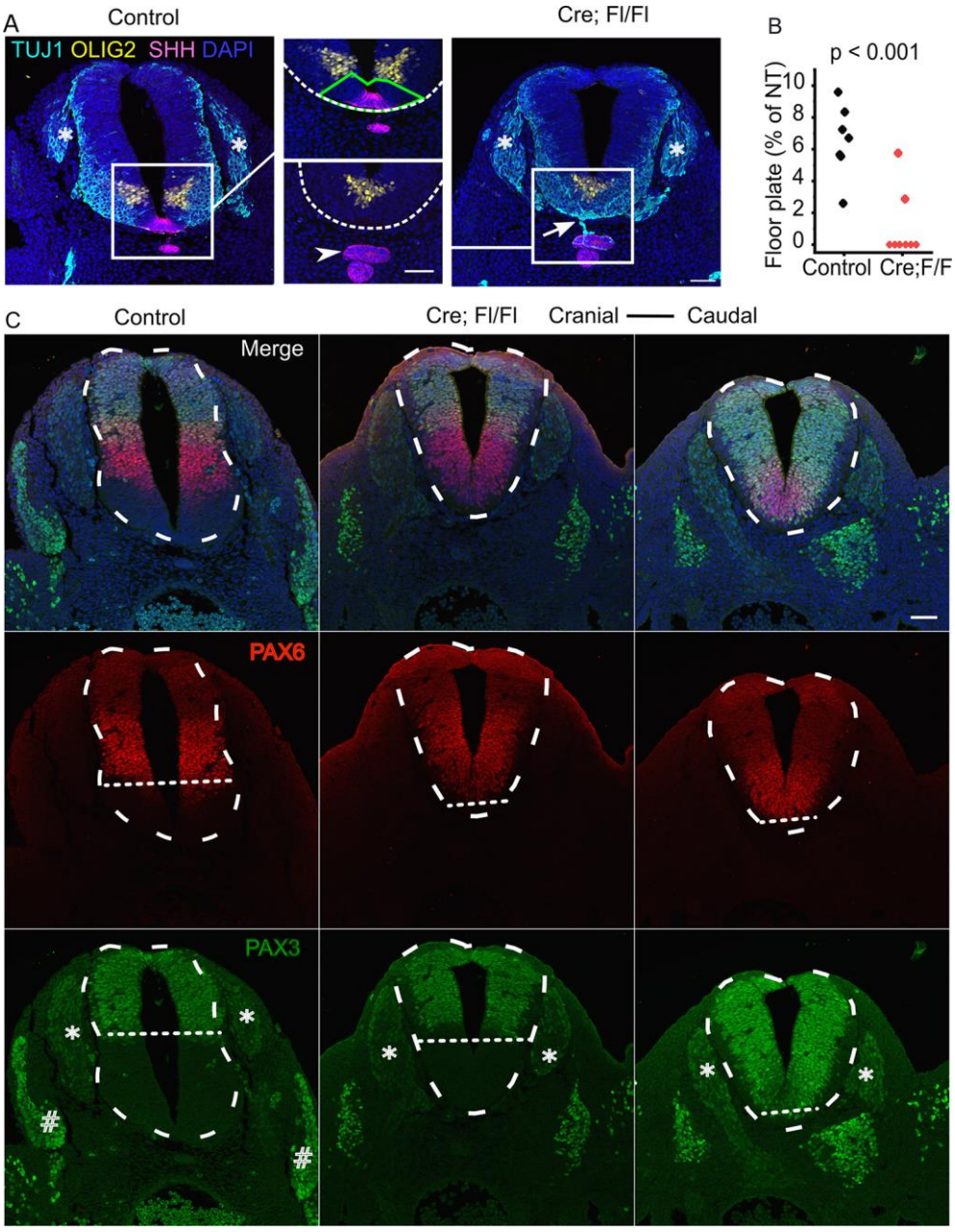

Fig. 6. Localized, progressive loss of ventral spinal progenitor domains precedes cystic dilation of the neural tube central canal in Fgfr1-disrupted embryos.

A. Immunofluorescent localization of the pMN marker OLIG2, floorplate marker SHH and neuron marker TUJ1 through the lumbar spinal cord of a control and Cre;Fl/Fl littermate collected at E11. White boxes indicate the regions in the insert, dashed white lines border the ventral neural tube, green polygon indicated the region ventral to the OLIG2 domain

quantified in B, * indicate dorsal root ganglia, arrowhead indicates ectopic Shh-expressing tissue, arrow indicates TUJ1-positive projection from the ectopic tissue. Scale bars = 50 µm.

B. Quantification of the portion of the neural tube ventral to the OLIG2 domain ('floor plate') as a proportion of neural tube area in control and Cre;Fl/Fl embryos collected at E10.5 and sectioned between the hindlimb buds.

C. Immunofluorescent localization of the intermediate neural progenitor marker PAX6 and dorsal/neural crest marker PAX3 in E11.5 embryos. Note PAX3 also labels cells in the neural crest-derived dorsal root ganglia (*) and somite-derived dermomyotome (#). Dashed white lines outline the neural tube, dotted lines indicate the ventral extent of each domain. Serial sections in the Cre;Fl/Fl embryos are ~50 µm apart. Scale bar = 50 µm.

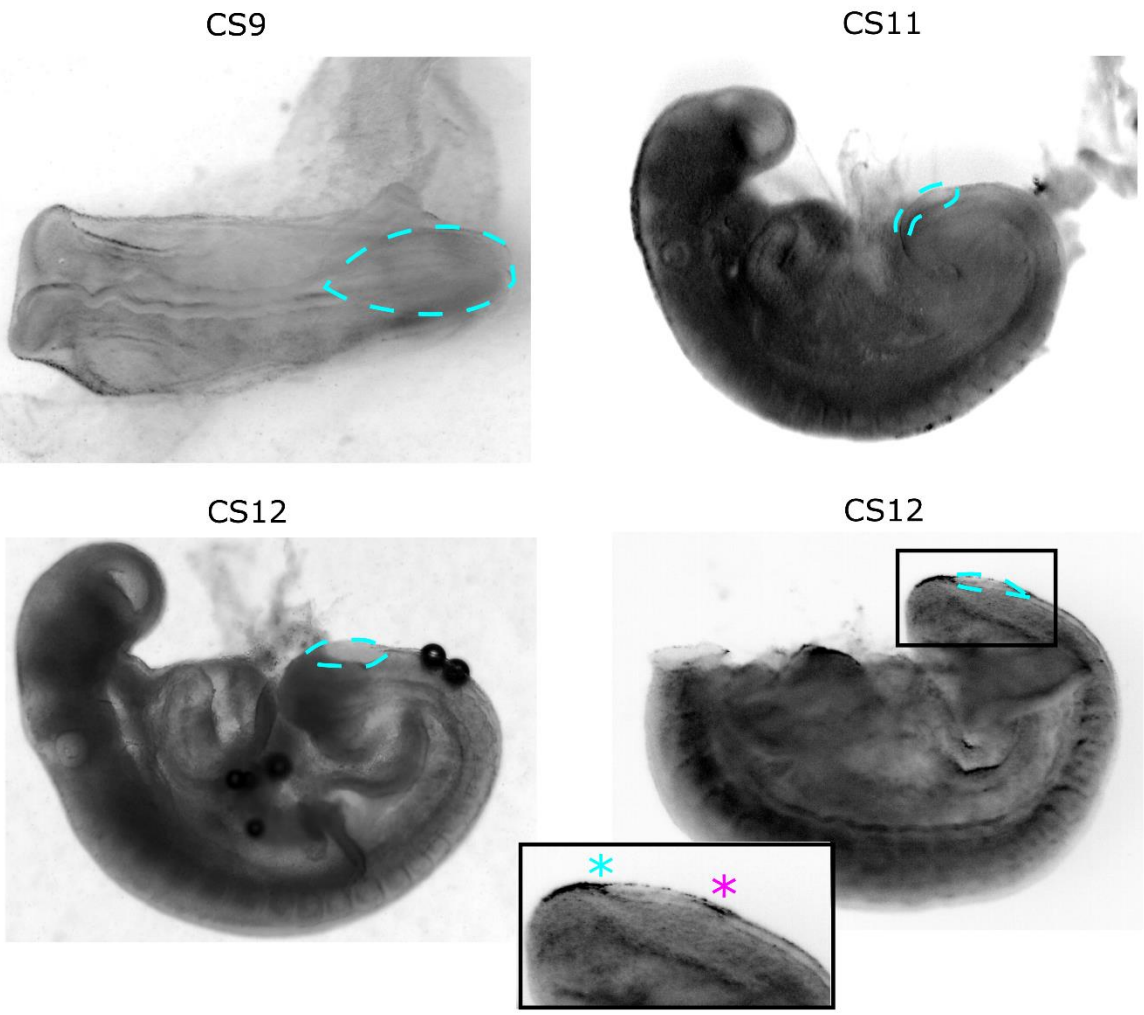

Fig. S1. Human PNPs have an elliptical morphology suggestive of Closure 5 formation at late stages of closure.

Brightfield images of human embryos at the Carnegie Stages (CS) indicated. The dashed cyan line annotates the posterior neuropore, which at CS9-11 has a spade-like morphology. By CS12, the human PNP has acquired an elliptical shape and the anatomy of the caudal extremity suggests formation of Closure 5 (cyan asterisk). The magenta asterisk indicates the rostral-to-caudal zippering point.

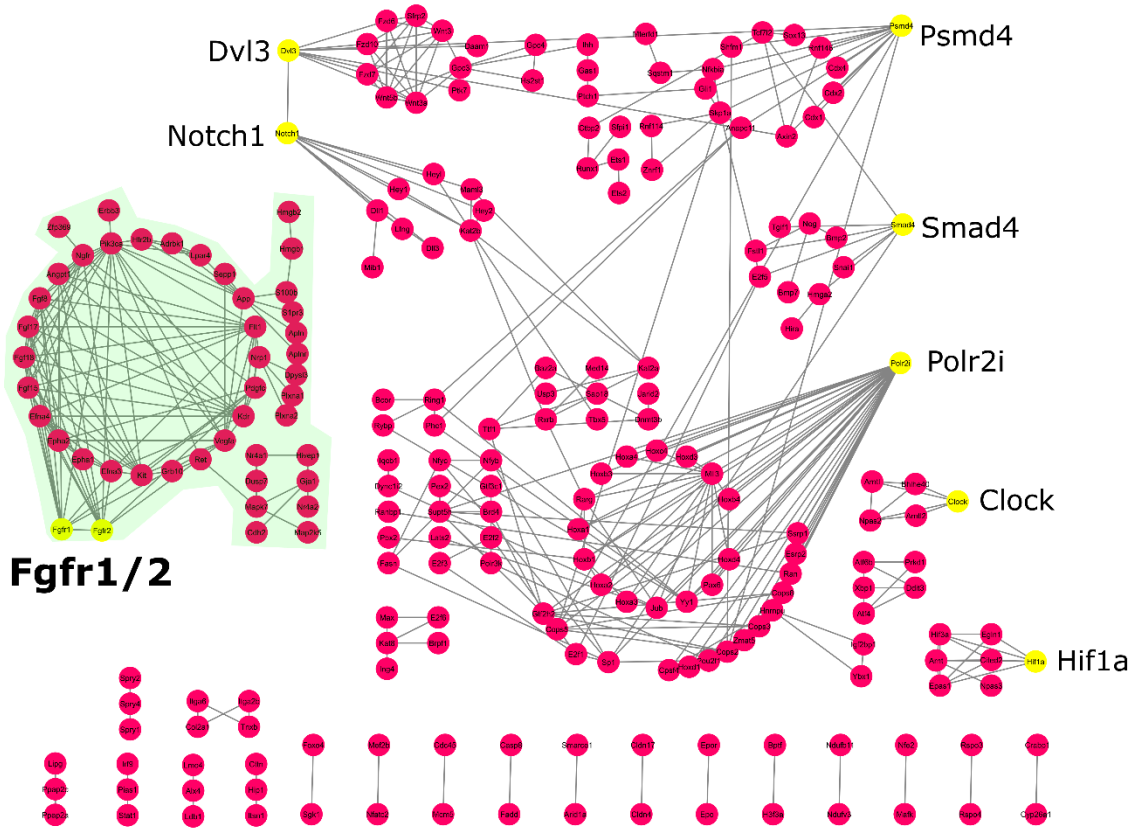

Fig. S2. FGF pathway components are known to be robustly expressed in the tissue region where Closure 5 forms.

523 genes known to be expressed in the region of Closure 5 formation (tail bud) between E9.5-E10.5 in mouse embryos were identified using the EMAGE gene expression database (http://www.emouseatlas.org/emage/)[1]. Genes whose protein products are known to interact with high confidence in reported experiments and curated databases were identified in StringDB[2]; non-interacting members were suppressed. The resulting network of interacting Closure 5-region genes was analyzed in Cytoscape[3] to identify sub-networks linked to nodes of interest (yellow, gene names annotated). Genes interacting with FGFR1 and 2 are indicated with green shading. Yellow nodes indicate genes related to specific pathway of interest. Results were obtained from bioinformatic analysis.

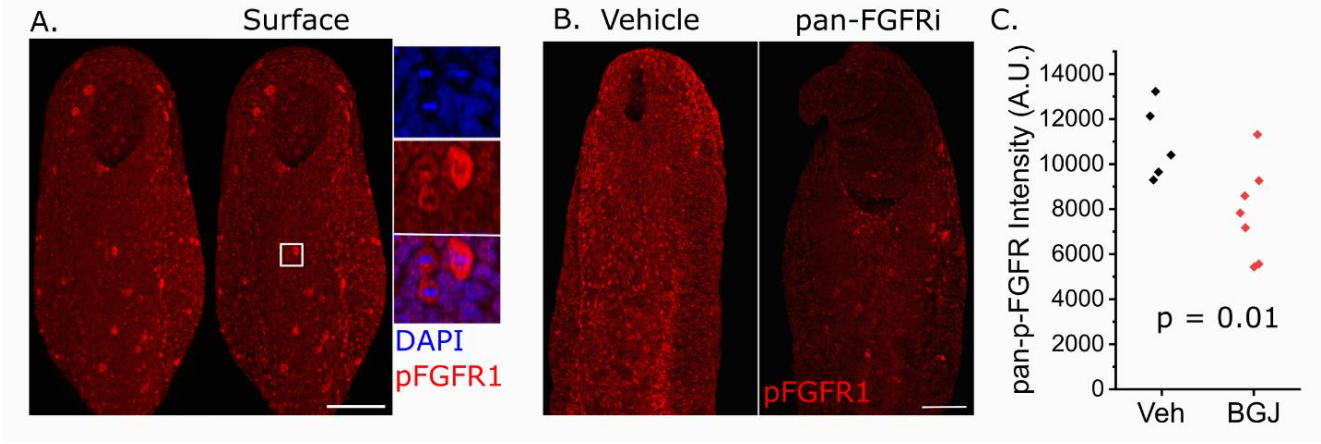

Fig. S3. Diminished p-FGFR1 following pharmacological antagonism.

A. Wholemount confocal image of a 28-somite embryo showing pFGFR1 immunolocalisation. The right panel is 'surface subtracted' to only show a 10 µm top surface, namely the surface ectoderm and apical neuroepithelium. Insert shows bright pFGFR1 labelling mitotic cells.

B. 'Surface subtracted' wholemount confocal images of embryos cultured in vehicle or pan-FGFR inhibitor for 24 hours. Scale bar = 100 µm.

C. pFGFR1 immunofluorescence intensity quantification in the 'surface subtracted' surface ectoderm of control and pan-FGFR inhibitor (BGJ) treated embryos. Surface subtraction was used to ensure the volume analysed is comparable between Z-stacks. P value by t-test.

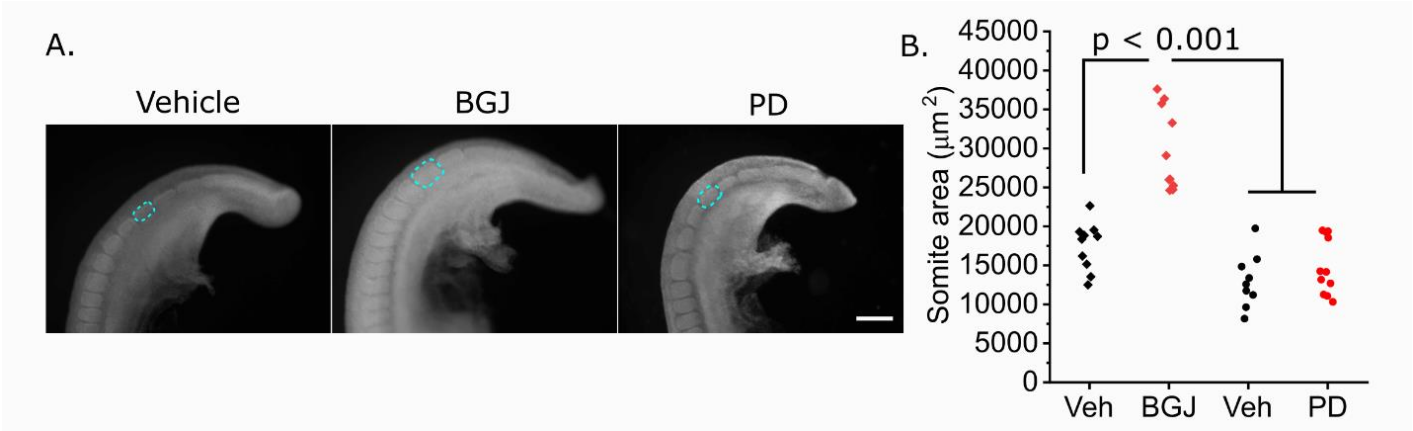

Fig. S4. Pan-FGFR inhibition increases somite size.

A. Fluorescent stereoscope images of DAPI-stained embryos treated for 24 hours with vehicle (DMSO), pan-FGFR inhibitor (BGJ) or FGFR1-targeting inhibitor (PD). Dashed cyan outlines indicate the penultimate somite. Scale bar = 225 µm.

B. Quantification of the projected area of the penultimate somite in FGFR-inhibited or vehicle-treated controls. The penultimate somite was chosen as this is more reliably visualized. Independent vehicle-treated littermate controls were included for both BGJ and PD cultures. Each point represents an embryo, p value by ANOVA with post-hoc Bonferroni.

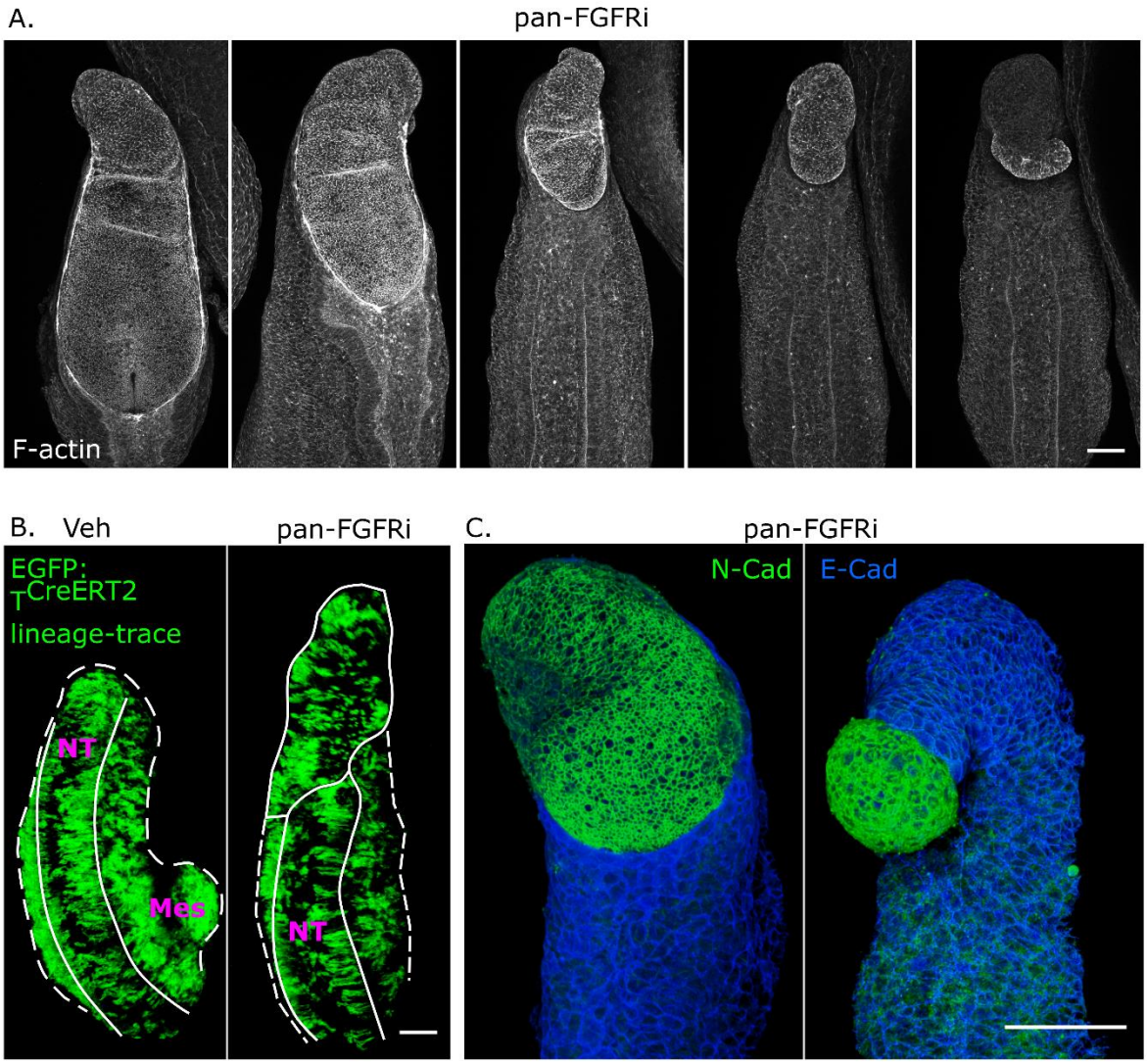

Fig. S5. Pharmacological inhibition of FGF signalling in cultured mouse embryos causes abnormal PNP closure.

A. Confocal images of phalloidin stained embryos cultured with pan-FGFR inhibitor for 24 hours.
B. 3D reconstructions of confocal-imaged vehicle and a pan-FGFR inhibitor treated embryo after 24 hours whole embryo culture. Neuromesodermal progenitors are lineage traced with *T*^{CreERT2} and continue to give rise to both neural tube (NT) and mesoderm (Mes) in both conditions.
C. 3D reconstructions of confocal-imaged embryos after 24 hour culture with pan-FGFR inhibitor. Immunolocalisation of E- and N-cadherin shows that the PNP overgrowth is neuroepithelial.

Scale bars = 100 µm.

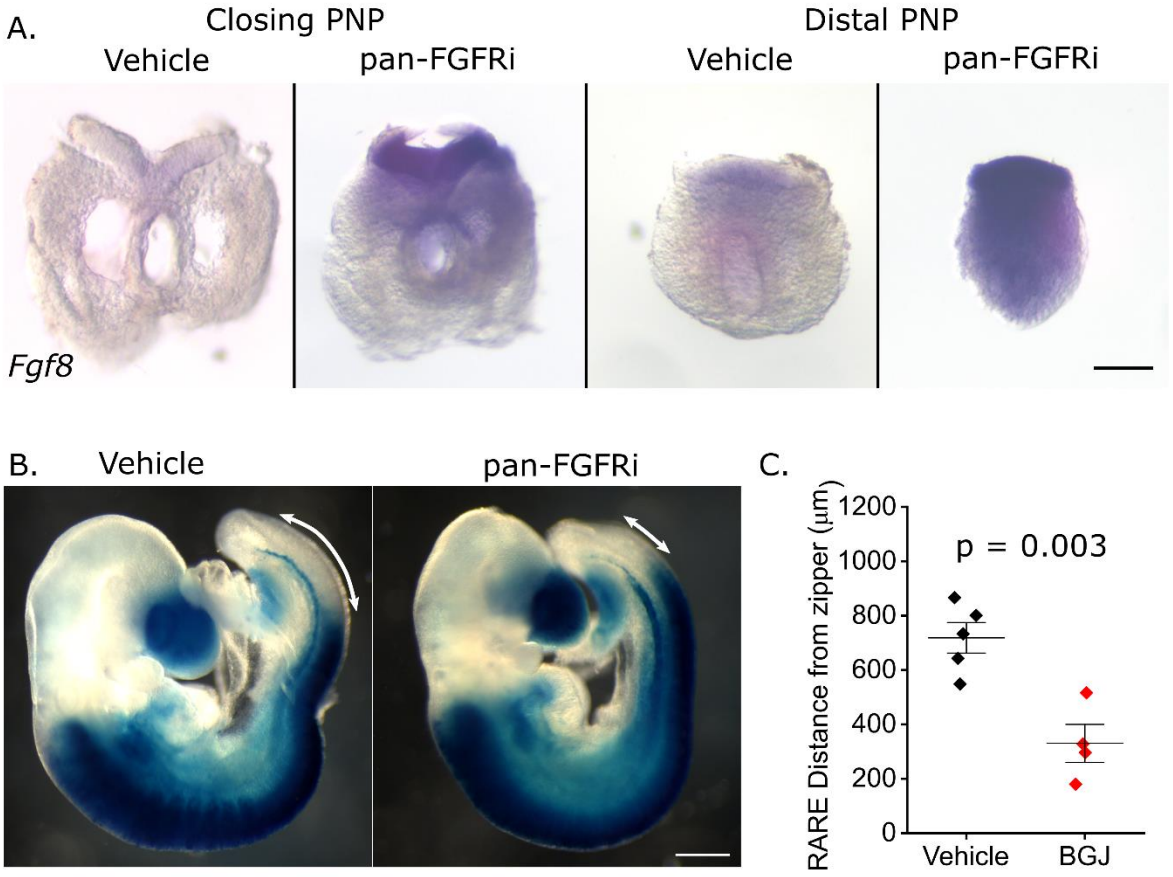

Fig. S6. Pan-FGFR inhibition for 8 hours increases *Fgf8* and causes caudal expansion of RARE signalling.

A. Vibratome sections of wholemount *Fgf8* in situ hybridisation in vehicle- and pan-FGFRi-treated embryos after 8 hours of whole embryo culture. Scale bar = 100 µm.
B. Brightfield images showing RARE-mediated LacZ expression domain in vehicle and pan-FGFRi-treated embryos after 24 hours of whole embryo culture. The double-headed white arrow indicates the distance between the RARE domain and the zippering point. Scale bar = 350 µm.
C. Quantification of RARE domain distance to the end of the zippering point in vehicle and pan-FGFRi (BGJ)-treated embryos after 8 hours of whole embryo culture. Points represent individual embryos.

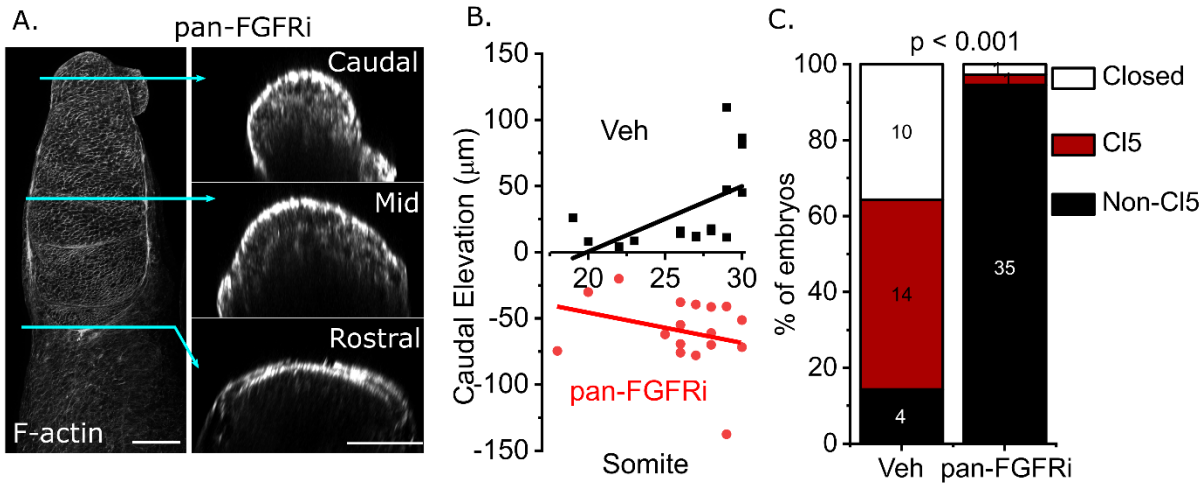

Fig. S7. Pharmacological inhibition of FGF signaling in cultured mouse embryos prevents neural fold elevation required for Closure 5 formation.

A. Confocal image of a phalloidin stained embryo after 24 hours culture with pan-FGFR inhibitor. The cyan arrows indicate the level of the optical cross-sections at the rostral, mid and caudal level. Scale bars = 100 μm.
B. Quantification of elevation at the caudal neural folds (90% of the PNP's length) in embryos at the indicated somite stages.
C. Quantification of the proportion of embryos collected at E10.5 with closed PNPs, open PNPs with Closure 5 morphology or open PNPs without Closure 5. Numbers indicate the number of embryos observed in each category.

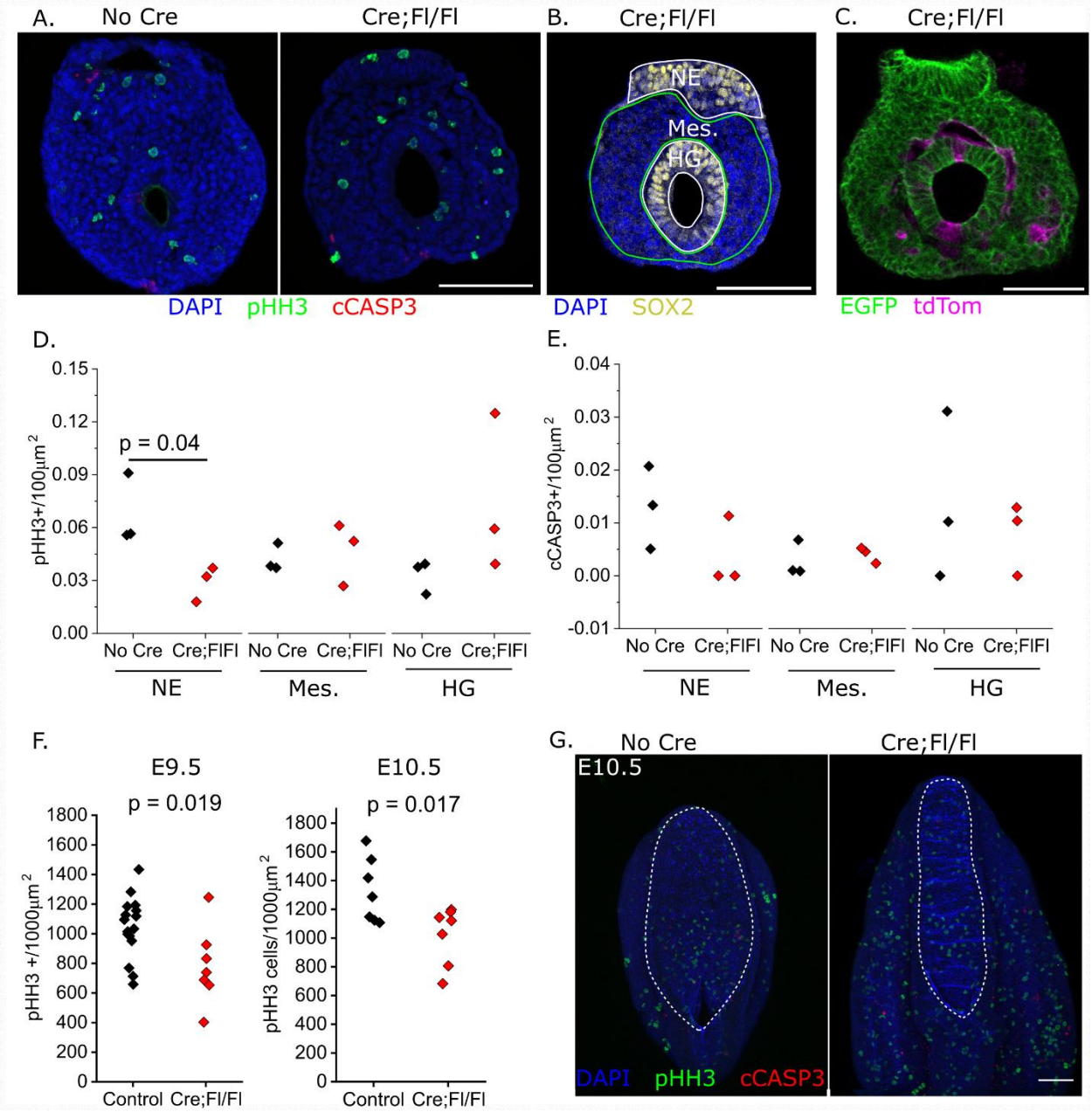

Fig. S8. *Fgfr1* deletion diminishes neuroepithelial proliferation.

A-B. Histological sections through the distal PNP of embryos at E10.5, when control embryos form Closure 5, immunofluorescently labelled to visualise the mitotic cell marker pHH3 and apoptosis marker cleaved caspase 3 (cCASP3). **B** shows annotation of the neuroepithelium (NE), mesoderm (Mes.) and hind-gut (HG) in an *Fgfr1*-deleted embryo immunolabelled for SOX2. Scale bars = 100 µm.

C. mTmG lineage tracing showing *Cdx2*^{Cre}-recombined (EGFP) and unrecombined (tdTom) cells in the distal tailbud of an E10.5 Cre;Fl/Fl embryo illustrating extensive lineage-tracing of most cells in this tissue. Scale bar = 100 µm.

D-E. Quantification of the number of proliferating or apoptotic cells per area in the NE, mesoderm or HG. Points represent individual embryos (n = 3 embryos per genotype).

F. Quantification of the number of mitotic cells per area of exposed neuroepithelium in control and Fgfr1-deleted embryos collected at E9.5 or E10.5 (embryos with closed PNPs were excluded). Points represent individual embryos.

G. Wholemount immunofluorescent images showing proliferating and apoptotic cells in control and Fgfr1-deleted embryos at E10.5. The dashed white line indicates the exposed neuroepithelium. Scale bar = 100 µm.

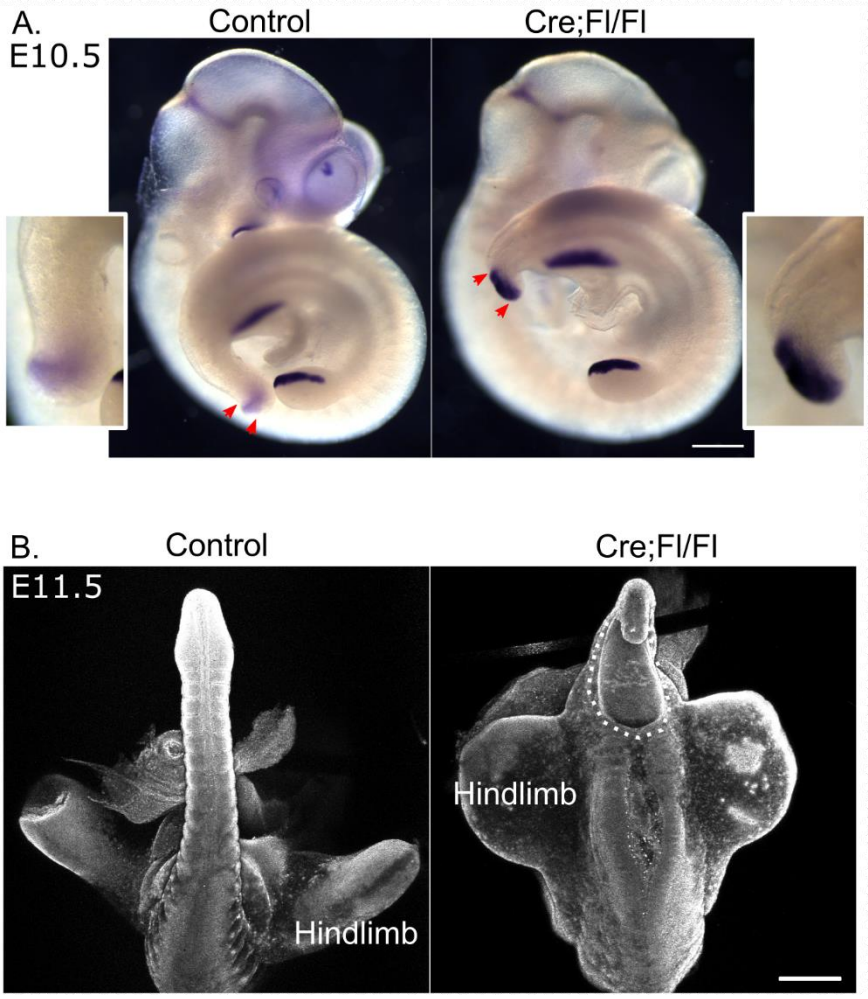

Fig. S9. *Fgf8* expression and late open neuropores in embryos with caudally-deleted *Fgfr1*.

A. Wholemount *Fgf8* in situ hybridisation in control and littermate Cre;Fl/Fl embryos. Arrowheads indicate the tailbud *Fgf8* domain, shown in the insets. Scale bar = 300 µm.

B. Reflection images of control and Cre;Fl/Fl littermates collected at E11.5. The dotted white line encircles the open lesion at the caudal end of the body axis. Scale bar = 500 µm.

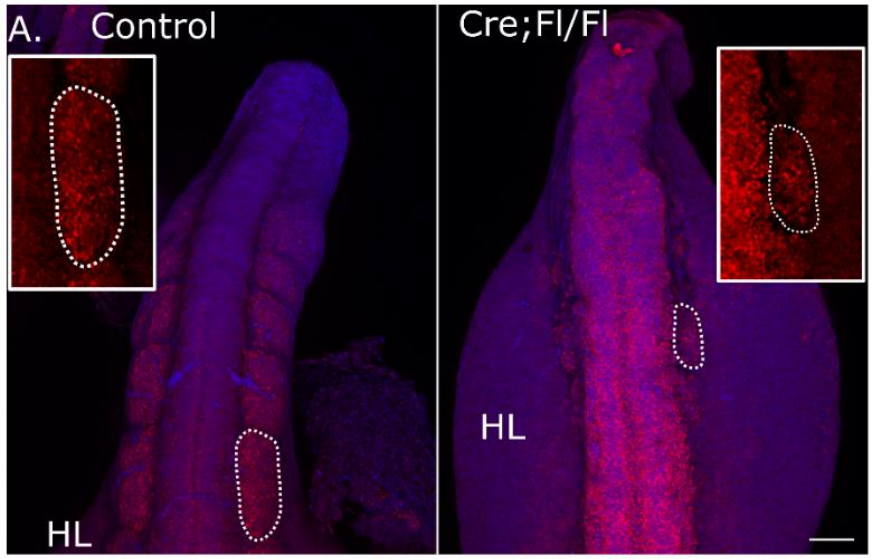

RALDH2 DAPI

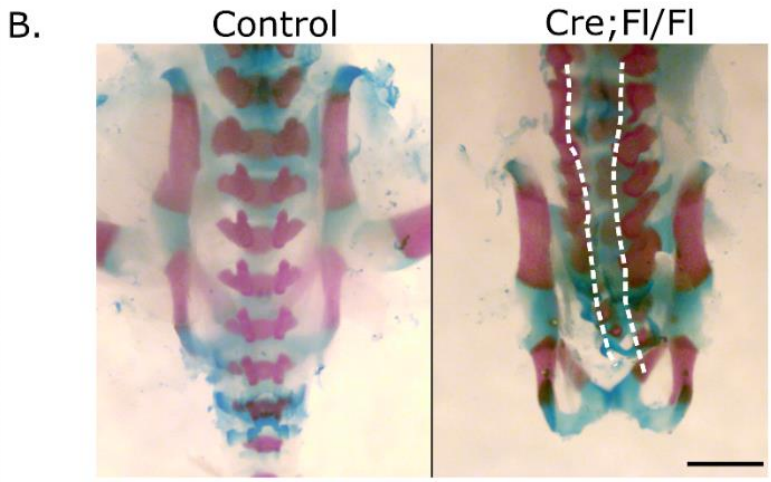

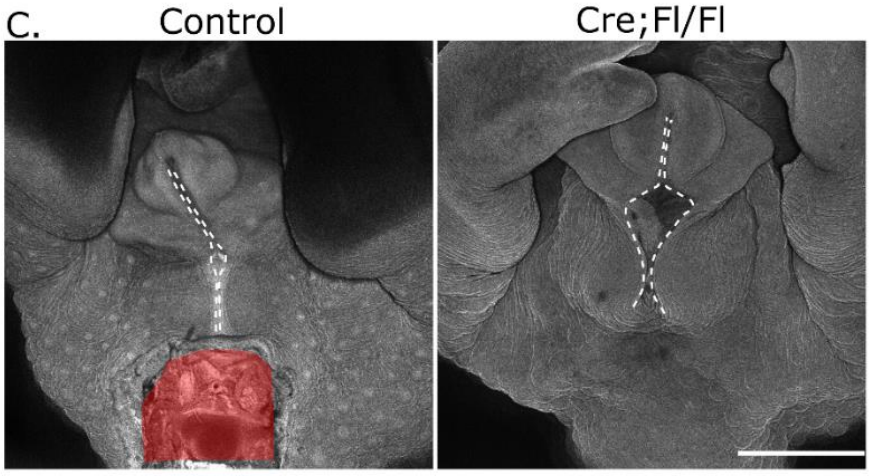

Fig. S10. Non-neuroepithelial abnormalities in embryos with caudally-deleted *Fgfr1*.

A. Wholemount immunofluorescent visualization of RALDH2 in an E10.5 control and littermate Cre;Fl/Fl embryo. Inserts show magnified views of a somite in each embryo (dashed lines). HL = hindlimbs, scale bar = 100 µm.
B. Whole-mount skeletal staining with Alcian blue and Alizarin red of control and Cre;Fl/Fl P1 pups from the same litter. Dashed white lines indicate bifid neural arches. Scale bar = 850 µm.
C. Reflection images of control and Cre;Fl/Fl littermates collected at E16.5. The dotted line annotates the perineum, which is fused in control and partially open in the mutant. Red area shows the tail base, which was cut to enable imaging of underlying structures in the control fetus. Scale bar = 1 mm.

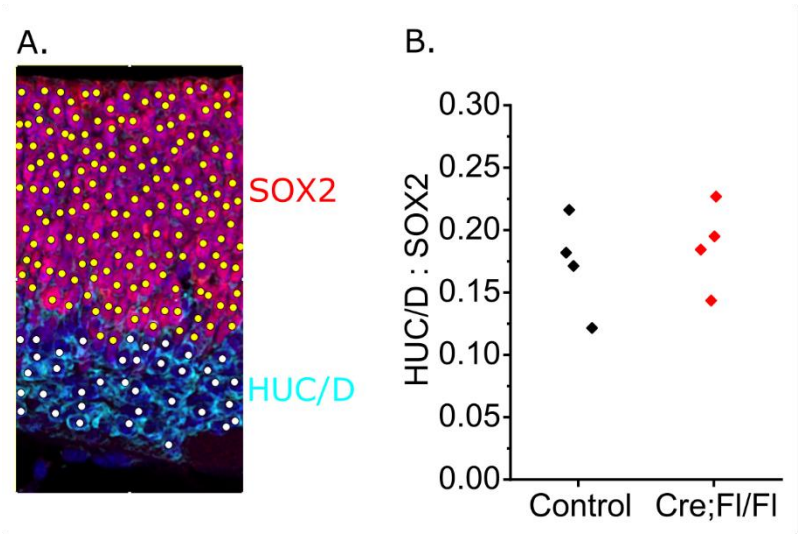

Fig. S11. *Fgfr1* disruption does not diminish neurogenesis in the distal spine.

A. Representative image of a 100 µm length of the lateral neural tube stained and imaged equivalently to embryos in Figure 5G. Yellow dots indicate SOX2-bright cells, white dots indicate HUC/D-bright cells.
B. Quantification of the ratio of HUC/D to SOX2 bright cells along 100 µm lengths of the lateral neural tube in control and *Fgfr1*-disrupted embryos. Points represent individual embryos.

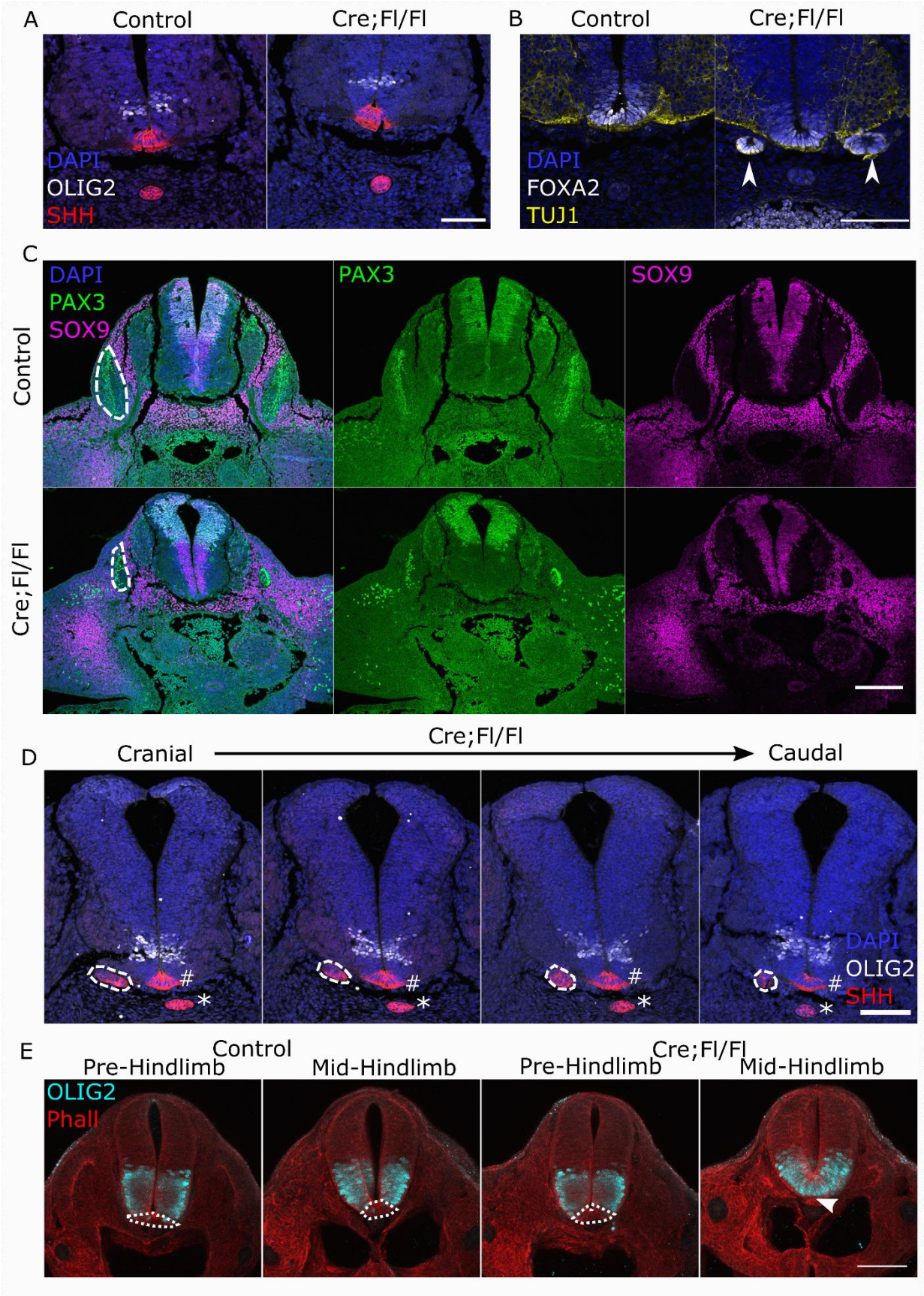

Fig. S12. Caudal *Fgfr1* deletion causes localized progenitor domain abnormalities.

A-C Immunofluorescent localization of neuronal progenitor markers through the lumbar spinal cord of control and Cre;Fl/Fl littermates collected at E11 showing: A) pMN marker OLIG2 and floor plate and notochord marker SHH. B) Post-mitotic neuronal marker Tuj1 and floor plate marker FOXA2. The arrowheads indicate ectopic FOXA2 foci in the Cre;Fl/Fl embryo. C) Dorsal/neural crest marker PAX3 and neuroepithelial/neural crest marker SOX9. The dashed line encircles the dermomyotome which is markedly reduced in the Cre;Fl/Fl embryo. Scale bars A,B = 100 µm, C = 200 µm.

D. Serial sections through the lumbar spinal cord of a Cre;Fl/Fl embryo collected at E11 and stained for OLIG2 and SHH. SHH stains the floor plate (#), notochord (*) and ventral ectopic clusters encircled by a dotted line. Scale bar = 100 µm.

E. Sections at pre- and mid-hindlimb level of control and Cre;Fl/Fl littermates collected at E10.5. The OLIG2 negative floor plate (dotted line), disappears at the mid-hindlimb level of the mutant (white arrowhead). Scale bar = 100 µm.

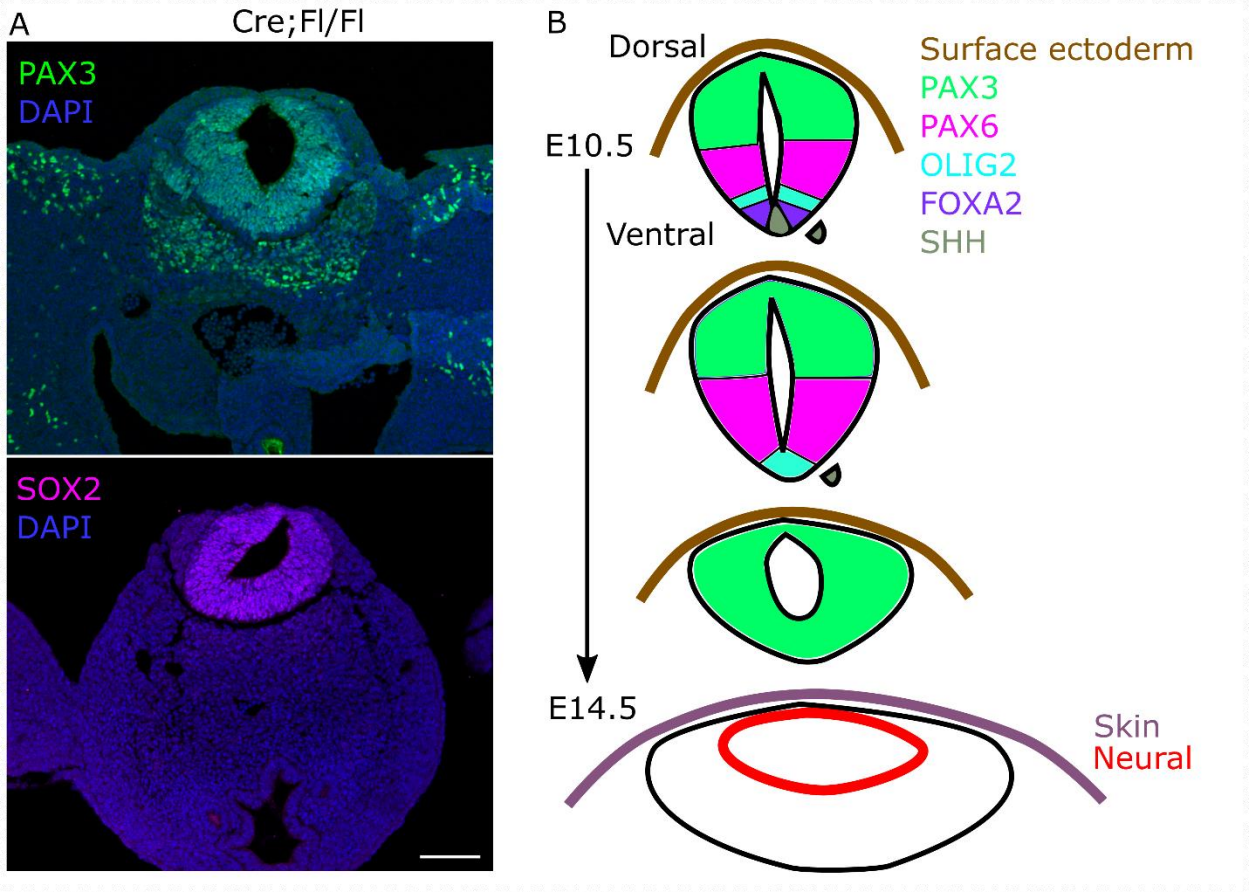

Fig. S13. Neural tube dorsalization precedes its dysmorphology and central canal dilation in *Fgfr1*-disrupted embryos.

A. Hindlimb level section through a Cre;Fl/Fl embryo collected at E11.5. The neural tube lumen is circular and stains positive for SOX2 and PAX3 throughout. Scale bar = 200 µm.

B. Schematic representation showing the progressive neural tube dorsalisation after caudal deletion of *Fgfr1* in Cre;Fl/Fl embryos. Ectopic clusters of SHH and FOXA2 at E10.5 precede loss of ventral progenitor domains. This leads to ventral expansion of PAX3 and PAX6 from E11.5, which finally encircle the neural tube lumen. Central canal dilation produces a terminal myelocystocele-like phenotype at E14.5.

Supplementary References

1 Richardson, L. *et al. Nucleic Acids Res* **42**, D835-844, doi:10.1093/nar/gkt1155 (2014).
2 von Mering, C. *et al. Nucleic Acids Res* **33**, D433-437, doi:10.1093/nar/gki005 (2005).
3 Shannon, P. *et al. Genome Res* **13**, 2498-2504, doi:10.1101/gr.1239303 (2003).